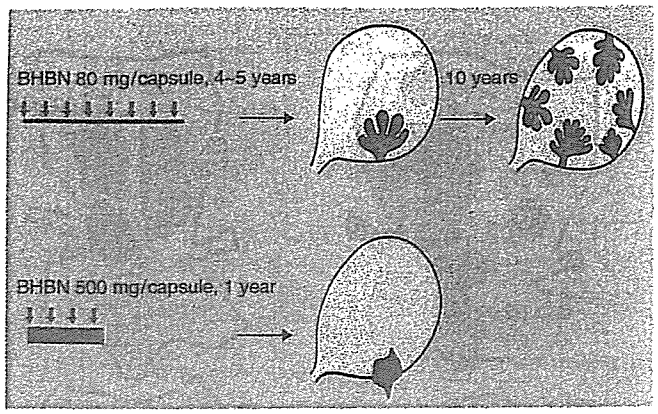

Fig. 5. Development and progression of papillary and nodular carcinomas depending on the concentration and period of administration of *N*-butyl-*N*-(4-hydroxybutyl) nitrosamine (BHBN) in female dogs.[34] (Reproduced with permission from Medical view Co., T. Kakizoe, Development and Progression of Bladder Cancer, 1995.)

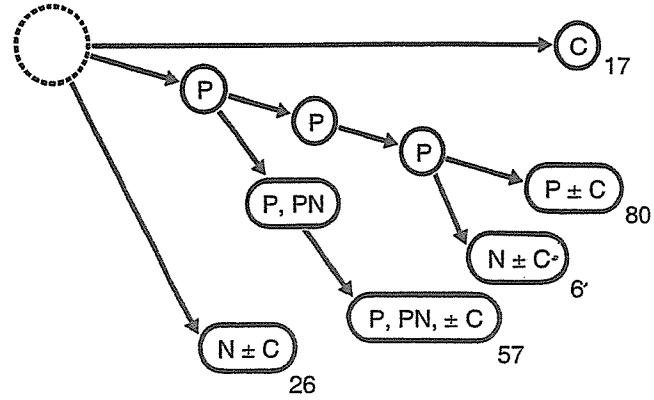

Fig. 6. Conceptual progression routes of papillary (P), papillonodular (PN) and nodular (N) carcinoma, and carcinoma *in situ* (C), in 186 cystectomized specimens examined by step-sectioning.[35]

as P and P + C. Fifty-seven cases featured apparent early changes from P to a mixture of P and N, whereas six showed late development of N with repeated recurrence of P. The findings thus indicated some N to have developed from P as more anaplastic cell populations within a pre-existing low-grade lesion, whereas others arose directly *de novo* from C (Fig. 6). Topographic relationships between P and N in the pT3 group are illustrated in Fig. 7. Figure 8 demonstrates findings for patients having a previous history of repeated recurrence of papillary carcinomas treated by TUR. At the time of cystectomy, all the cystectomized specimens showed a variable degree of coexistence of P, N and C.

Molecular pathways of urothelial carcinogenesis

With papillary superficial and nodular invasive carcinomas, there appear to be differences in molecular pathways as well

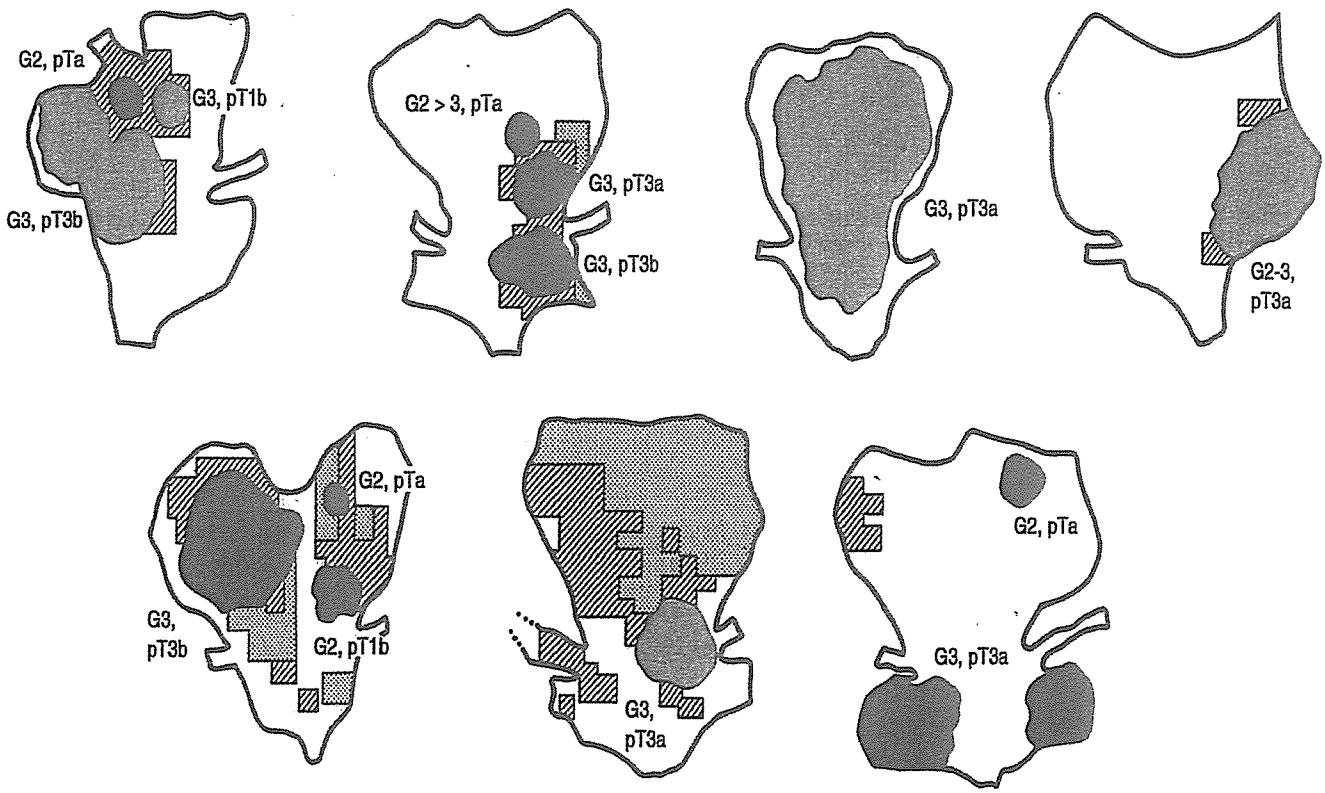

Fig. 7. Cases of pT3 cystectomized specimens indicating coexistence of papillary (P; blue), papillonodular (PN; yellow) and nodular (N; red) carcinoma together with oblique line area (C) and shaded area (dysplasia).[35]

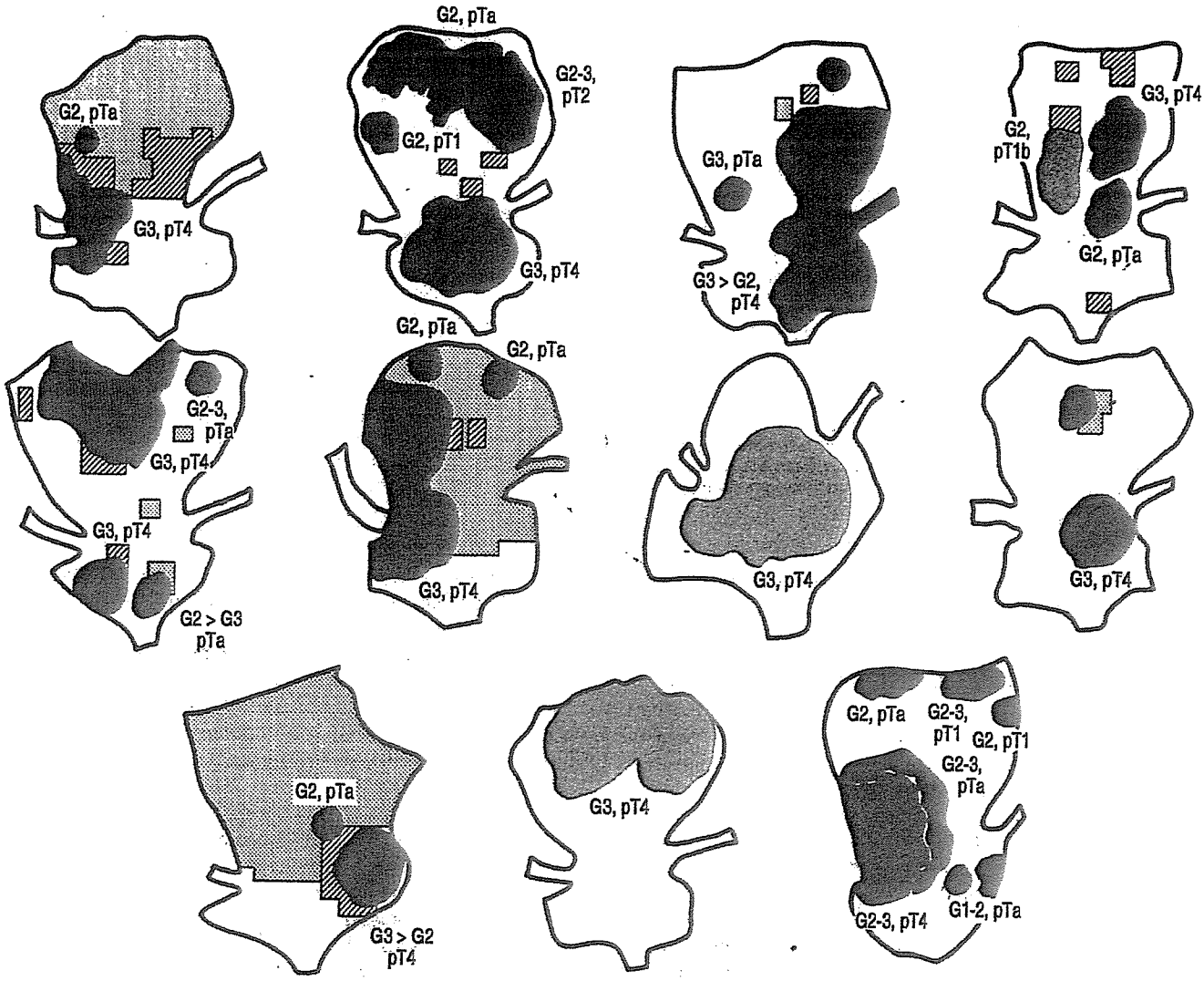

Fig. 8. Eleven cases of cystectomized specimens having histories of multiple transurethral resection for papillary recurrent carcinomas showing variety of stages and morphology in a single bladder.[35]

as morphology[36–38] (Fig. 9). The most common genetic alterations in low-grade papillary urothelial carcinomas are LOH of chromosome 9 and activating mutations of fibroblast growth factor receptor 3 (FGFR3).[39,40] Over 70% of low-grade papillary carcinoma exhibit FGFR3 mutations, but only 10–20% of high-grade invasive carcinomas have FGFR3 mutations, implying a key role for FGFR3 together with mutations of 9p and 9q, specifically for the induction of low-grade papillary carcinomas. Invasive carcinoma is frequently associated with p53 mutations.[41–43]

In addition to the above-mentioned genomic abnormalities associated with urothelial carcinoma, epigenetic alterations also occur during urothelial carcinogenesis. Almost all cells in the human body contain the same sequence of DNA, but cells in different organs during different developmental stages express different genes by epigenetic control of cellular function. This expression control of DNA is achieved by DNA methylation, chromatin structure and transcription factors. DNA can be methylated at cytosine residues adjacent to guanine residues (CpG) and CpG sites are distributed non-randomly throughout the genome, being found as islands in the promoter and exonic regions. Inactivation of tumor suppressor genes is known to occur via promoter hypermethylation, frequently due to DNA methyltransferase 1 (DNMT1). Expression of DNMT1 is increased in tumors and even during the precancerous stages of the urothelium with the development of flat carcinomas *in situ*.[44] Hypermethylation in urothelial carcinogenesis has also been observed in the promoter region of the E-cadherin gene, indicating an association with carcinoma *in situ* and detachment of cells or clusters of carcinoma cells in the urine.[45]

Development and progression of urothelial carcinoma

As is shown in Fig. 1, multifocal transitional cell carcinomas may develop in any region of the urinary tract, from the renal pelvis/ureter to the bladder/urethra.[4,46] Whereas upper urinary

doi: 10.1111/j.1349-7006.2006.00264.x

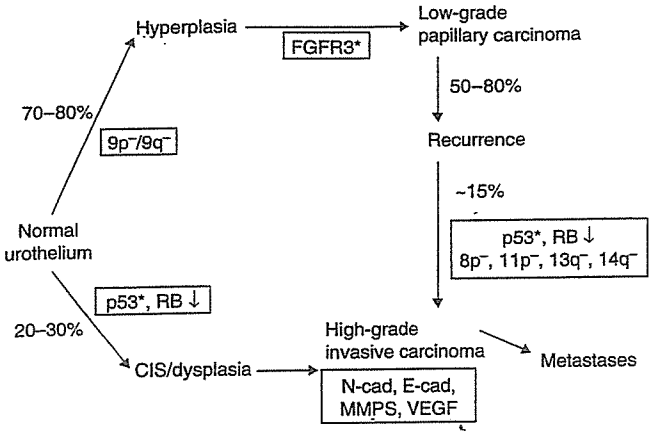

Fig. 9. Presumed molecular pathways of development of papillary and nodular carcinoma. (Modified from Wu.[38]) CIS, carcinoma *in situ*; FGFR3, fibroblast growth factor receptor 3; MMPS, matrix metal proteinases; RB, retinoblastoma gene; VEGF, vascular endothelial growth factor.

tract carcinomas occur infrequently after transurethral management of bladder carcinomas, the incidence is much greater in patients with vesico-ureteral reflux,[10] suggesting seeding or implantation of primary urothelial carcinoma cells after spread via the urine rather than field cancerization. In addition, recent molecular analyses using X-chromosome inactivation,[23] p53 mutation,[24–28] LOH[27,28] and comparative genomic hybridization[29] have provided compelling evidence that multifocal urothelial carcinomas are monoclonal in origin, despite some discrepancies.[30,31]

Comparing the basic morphological patterns of urothelial carcinomas, namely low-grade, superficial papillary carcinomas and high-grade, invasive nodular carcinomas, these two patterns of urothelial carcinomas are clearly separated in rats[32] and mice.[33] However, in dogs,[34] papillary carcinomas and nodular carcinomas can both be induced, depending on the concentration and period of carcinogen administration. In humans, papillary carcinomas and nodular carcinomas may originally develop separately, but coexistence of the two types is occasionally observed in a single bladder together with dysplasia and carcinoma *in situ*.[35] During the process of repeated recurrence, progression from papillary carcinoma to nodular carcinoma may be observed and molecular analysis of bladder carcinogenesis indicates the presence of two pathways: LOH of 9p/9q loss and FGFR3 mutation resulting in papillary carcinoma, and if p53 mutation occurs, nodular carcinoma. If p53 mutations occur initially, nodular carcinoma develops via dysplasia and carcinoma *in situ*. The available data clearly indicate that multiple genetic alterations are associated with the development and progression of bladder cancer.[36–38]

In the normal-appearing mucosa of the renal pelvis, ureter and bladder, dysplasia and carcinoma *in situ* may be frequently observed.[46] As mucosal dysplasia is not malignant, a derivation by implantation from primary carcinomas is not conceivable. In normal-appearing mucosa in remote areas from tumors, p53 mutation may be observed.[27] Intraepithelial spread[27,28] has been proposed as an explanation but this would appear unlikely. The phenomenon of coexistence of dysplasia, carcinoma *in situ* and p53 mutation in normal-appearing mucosa can be far more readily explained by the field cancerization theory. Differences in growth patterns of papillary and nodular carcinomas, and carcinoma *in situ*, as well as in cellular polarity and grade of malignancy make a single origin by seeding unreasonable. Finally, on detailed analysis of recurrent patterns of papillary carcinomas after TUR with or without intravesical instillation therapy, Akaza *et al.* concluded that recurrence patterns are biphasic, with an initial peak due to seeding or implantation of cancer cells during therapy and a second peak due to a new tumor occurrence from a background of field changes.[47] Thus, multifocal bladder recurrence of urothelial carcinomas is due to a combination of seeding and field changes. This is directly relevant to the condition for reconstruction of the urinary tract after cystectomy, inhibition and control of multiple recurrences after TUR, and the frequency and timing of follow-up for upper tract malignancies after treatment of bladder carcinoma. However, such clinical issues will be covered elsewhere.

References

1 Koss LG. *Tumors of the Urinary Bladder*. Washington DC: Armed Forces Institute of Pathology, 1975.
2 Parkin DM, Bray F, Ferlay J, Pisani P. Estimating the world cancer burden: Globocan 2000. *Int J Cancer 2001* 1998; **94**: 153–6.
3 *Cancer Incidence in Sweden 1998*. Stockholm, Sweden: The National Board of Health and Welfare, 1998.
4 Kakizoe T, Tobisu K, Tanaka Y *et al.* Development of multiple transitional cell carcinomas in the urinary tract. *Jpn J Clin Oncol* 1991; **21**: 110–14.
5 Studer UE, Hautmann RE, Hohenfellner M *et al.* Indication for continent diversion after cystectomy and factors affecting long-term result. *Urol Oncol* 1998; **4**: 172–80.
6 Coloby P, Kakizoe T, Tobisu K, Sakamoto M. Urethral involvement in female bladder cancer patients: mapping of 47 consecutive cystourethrectomy specimens. *J Urol* 1994; **152**: 1438–42.
7 Kirkali Z, Tuzel E. Transitional cell carcinoma of the ureter and renal pellvis. *Crit Rev Oncol Hematol* 2003; **47**: 155–60.
8 Palon J, Farina LA, Villavicencio H, Vicente J. Upper tranct urothelial tumor after transurethral resection for bladder tumor. *Eur Urol* 1992; **21**: 110–14.
9 Canales BK, Anderson JK, Premoli J, Slaton JW. Risk factors for upper tract recurrence in patients undergoing long-term surveillance for stage Ta bladder cancer. *J Urol* 2006; **175**: 74–7.
10 De Torres Mateos JA, Banus Gassol JM, Palou Redorta J, Morote Robles J. Vesicorenal reflux and upper urinary tract transitional cell carcinoma after transurethral resection of recurrent superficial bladder carcinoma. *J Urol* 1987; **138**: 49–51.
11 Kang CH, Yu TJ, Hsieh HH, Yang JW, Shu K, Huang CC. The development of bladder tumors and contralateral upper urinary tract tumors after primary transitional cell carcinoma of the upper urinary tract. *Cancer* 2003; **98**: 1620–6.
12 Charbit L, Gendrean MC, Mee S, Çukier J. Tumors of the upper urinary tract: 10 years of experience. *J Urol* 1991; **146**: 1243–6.
13 Harris AL, Neal DE. Bladder cancer-field versus clonal origin. *N Engl J Medical* 1992; **326**: 759–61.
14 Carcia SB, Park HS, Novelli M, Wright NA. Field cancerization, clonality, and epithelial stem cells: the spread of mutated clones in epithelial sheets. *J Pathol* 1999; **187**: 61–81.
15 Slaughter DP, Southwick HW, Smejkal W. Field cancerization in oral stratified squamous epithelium; clinical implications of multicentric origin. *Cancer* 1953; **6**: 963–8.
16 Scholes AG, Woolgar JA, Boyle MA, Brown JS. Synchronous oral carcinomas: independent or common clonal origin? *Cancer Res* 1998;

58: 2003–6.
17 Sozzi G, Miozzo M, Pastorinou U *et al.* Genetic evidence for an independent origin of multiple preneoplastic and neoplastic lung lesions. *Cancer Res* 1995; **55**: 135–40.
18 Bedi GC, Westra WH, Gabrielson E, Koch W, Sindransky D. Multiple head and neck tumors: evidence for a common clonal origin. *Cancer Res* 1996; **56**: 2484–7.
19 Noguchi S, Aihara T, Koyama H, Motomura K, Inaji H, Imaoka S. Discrimination between multicentric and multifocal carcinomas of the breast through clonal analysis. *Cancer* 1994; **74**: 872–7.
20 Abeln EC, Kuipers-Dijkshoorn NJ, Berns EM, Henzen-Logmans SC, Fleuren GJ, Cornelisse CJ. Molecular genetic evidence for unifocal origin of advanced epithelial ovarian cancer and for minor clonal divergence. *Br J Cancer* 1995; **71**: 1330–6.
21 Larson AA, Liao SY, Stanbridge EJ, Cavenee WK, Hampton GM. Genetic alterations accumulate during cervical tumorigenesis and indicate a common origin for multifocal lesions. *Cancer Res* 1997; **57**: 4171–6.
22 Franklin WA, Gazdar AF, Haney J, Wistuba II. Widely dispersed p53 mutation in respiratory epithelium: A novel mechanism for field carcinogenesis. *J Clin Invest* 1997; **100**: 2133–7.
23 Sidransky D, Frost P, von Eschenbach A, Oyasu R, Preisinger AC, Vogelstein B. Clonal origin of bladder cancer. *N Engl J Med* 1992; **326**: 737–40.
24 Lunec J, Challen C, Wright C, Mellon K, Neal DE. c-erb B-2 amplification and identical p53 mutations in concomitant transitional carcinomas of renal pelvis and urinary baldder. *Lancet* 1992; **339**: 439–40.
25 Habuchi T, Takahashi R, Yamada H, Kakehi Y, Sugiyama T, Yoshida O. Metachronous multifocal development of urothelial cancers by intraluminal seeding. *Lancet* 1993; **342**: 1087–8.
26 Habuchi T. Origin of multifocal carcinomas of the bladder and upper urinary tract: molecular analysis and clinical implications. *Int J Urol* 2005; **12**: 709–16.
27 Stoehr R, Knuechel R, Boecker J *et al.* Histologic–genetic mapping by allele-specific PCR reveals intraurothelial spread of p53 mutant tumor clones. *Lab Invest* 2002; **82**: 1553–61.
28 Simon R, Eltze E, Schaefer KL *et al.* Cytogenetic analysis of multifocal bladder cancer supports a monoclonal origin and intraepithelial spread of tumor cells. *Cancer Res* 2001; **61**: 355–62.
29 Elmula IF, Gorunova L, Mandahl N *et al.* Cytogenetic monoclonality in multifocal uroepithelial carcinomas: evidence of intraluminal tumor seeding. *Br J Cancer* 1999; **81**: 6–12.
30 Cheng L, Gu J, Ulbright T *et al.* Precise microdissection of human bladder carcinomas reveals divergent tumor subclones in the same tumor. *Caner* 2002; **94**: 104–10.
31 Paiss T, Wohr G, Hautmann RE *et al.* Some tumors of the bladder are polyclonal in origin. *J Urol* 2002; **167**: 718–23.
32 Ito N. Early changes caused by *N*-buthyl-*N*-(4-hydroxybuthyl) nitrosamine in the bladder epithelium of different animal species. *Cancer Res* 1976; **36**: 2528–31.
33 Ohtani M, Kakizoe T, Sato S, Sugimura T, Fukushima S. Strain differences in mice with invasive bladder carcinomas induced by *N*-butyl-*N*-(4-hydroxybutyl) nitrosamine. *J Cancer Res Clin Oncol* 1986; **112**: 107–10.
34 Okajima E, Hiramatsu T, Motomiya Y *et al.* Urinary bladder tumors induced by *N*-butyl-*N*-(4-hydroxybutyl) nitrosamine in dogs. *Cancer Res* 1981; **41**: 1958–65.
35 Kakizoe T, Tobisu K, Takai K, Tanaka Y, Kishi K, Teshima S. Relationship between papillary and nodular transitional cell carcinoma in the human urinary bladder. *Cancer Res* 1988; **48**: 2293–303.
36 Spruck CH 3rd, Ohneseit PF, Gonzales-Zulueta M *et al.* Two molecular pathways to transitional cell carcinomas of the bladder. *Cancer Res* 1994; **54**: 784–8.
37 Woff EM, Liang G, Jones PA. Mechanisms of disease: genetic and epigenetic alterations that drive bladder cancer. *Nature Clin Pract Urol* 2005; **2**: 502–10.
38 Wu XR. Urothelial tumorigenesis: a tale of divergent pathways. *Nature Rev Cancer* 2005; **5**: 713–25.
39 Cappellen D, De Oliveria C, Ricol D *et al.* Frequent activating mutations of FGFR3 in human bladder and cervix carcinomas. *Naturel Genet* 1999; **23**: 18–20.
40 Rieger-Christ KM, Mourtzinos A, Lee PJ *et al.* Identification of fibroblast growth factor receptor 3 mutations in urine sediment DNA samples complements cytology in bladder tumor detection. *Cancer* 2003; **98**: 737–44.
41 Fujimoto K, Yamada Y, Okajima E *et al.* Frequent association of p53 gene mutation in invasive bladder cancer. *Cancer Res* 1992; **52**: 1393–8.
42 Hartmann A, Schlake G, Zaak D *et al.* Occurrence of chromosome 9 and p53 alterations in multifocal dysplasia and carcinoma *in situ* of human urinary bladder. *Cancer Res* 2002; **62**: 809–18.
43 Stein JP, Ginsberg DA, Grossfeld GD *et al.* Effect of p21WAF1/CIP1 expression on tumor progression in bladder cancer. *J Natl Cancer Inst* 1998; **90**: 1072–9.
44 Nakagawa T, Kanai Y, Saito Y, Kitamura T, Kakizoe T, Hirohashi S. Increased DNA methyltransferase 1 protein expression in human transitional cell carcinoma of the bladder. *J Urol* 2003; **170**: 2463–6.
45 Horikawa Y, Sugano K, Shigyo M *et al.* Hypermethylation of an E-cadherin (CDH1) promoter region in high grade transitional cell carcinoma of the bladder comprising carcinoma *in situ*. *J Urol* 2003; **169**: 1541–5.
46 Kakizoe T, Fujita J, Murase T, Matsumoto K, Kishi K. Transitional cell carcinoma of the bladder in patients with renal pelvic and ureteral cancer. *J Urol* 1980; **124**: 17–19.
47 Akaza H, Kurth KH, Hinotsu S *et al.* Intravesical chemotherapy and immunotherapy for superficial tumors: basic mechanism of action and future direction. *Urol Oncol* 1998; **4**: 121–9.

doi: 10.1111/j.1349-7006.2006.00264.x

Staging performance of carbon-11 choline positron emission tomography/computed tomography in patients with bone and soft tissue sarcoma: Comparison with conventional imaging

Ukihide Tateishi,[1,6] Umio Yamaguchi,[2] Testuo Maeda,[1] Kunihiko Seki,[3] Takashi Terauchi,[4] Akira Kawai,[2] Yasuaki Arai,[1] Noriyuki Moriyama[4] and Tadao Kakizoe[5]

[1]Diagnostic Radiology, [2]Orthopedic Division, and [3]Division of Clinical Pathology, National Cancer Center Hospital, [4]Division of Cancer Screening, and [5]President, National Cancer Center, Research Center for Cancer Prevention and Screening, Japan

(Received May 17, 2006/Revised June 21, 2006/Accepted June 26, 2006/Online publication August 14, 2006)

The present study was conducted to compare the diagnostic accuracy between carbon-11 choline (^{11}C-choline) positron emission tomography (PET)/computed tomography (CT) and conventional imaging for the staging of bone and soft tissue sarcomas. Sixteen patients who underwent ^{11}C-choline PET/CT prior to treatment were evaluated retrospectively for staging accuracy. Conventional imaging methods consisted of ^{99m}Tc-hydroxymethylene diphosphonate bone scintigraphy, chest CT and magnetic resonance imaging of the primary site. The images were reviewed and a consensus was reached by two board-certified radiologists who were unaware of any clinical or radiological information using hard-copy films and multimodality computer platform. Tumor stage was confirmed by histological examination and/or by an obvious progression in number and/or size of the lesions on follow-up examinations. Reviewers examining both ^{11}C-choline PET/CT and conventional imaging classified T stage in all patients. Interpretation based on ^{11}C-choline PET/CT, the Node (N) stage was correctly diagnosed in all patients, whereas the accuracy of conventional imaging in N stage was 63%. Tumor Node Metastasis (TNM) stage was assessed correctly with ^{11}C-choline PET/CT in 15 of 16 patients (94%) and with conventional imaging in eight of 16 patients (50%). The overall TNM staging and N staging accuracy of ^{11}C-choline PET/CT were significantly higher than that of conventional imaging ($P < 0.05$). ^{11}C-choline PET/CT is more accurate than conventional imaging regarding clinical staging of patients with bone and soft tissue sarcomas. A whole body ^{11}C-choline PET/CT might be acceptable for imaging studies of tumor staging prior to treatment. (*Cancer Sci* 2006; 97: 1125–1128)

The general diagnostic tools for staging bone and soft tissue sarcomas are clinical examination, magnetic resonance imaging (MRI) and X-ray of the primary tumor site, chest X-ray or computed tomography (CT), and bone scintigraphy.(1)

Positron emission tomography (PET) with [18F]-fluoro-2-deoxy-D-glucose (FDG) has been used in the evaluation of patients with bone and soft tissue sarcomas for grading and therapy monitoring.(2–7) Most of these studies reveal that ^{18}FDG-PET is superior in the assessment of grading and therapy monitoring compared with conventional imaging.

Recently, carbon-11 choline (^{11}C-choline) has been introduced as a new oncological positron-emitting radiopharmaceutical for evaluation of a variety of malignant tumors.(8–11) Choline is an essential component of the cell membrane, and choline uptake may be via a choline-specific transporter protein.(12) Choline kinase, which catalyzes the phosphorylation of choline, is upregulated in malignant cells. Some studies have demonstrated additional gains in diagnostic accuracy using ^{11}C-choline.(13) ^{11}C-choline uptake is significantly higher in malignant tumors than in benign tumors and correlates well with the degree of ^{18}FDG accumulation with the lesion, while the high background activity owing to excretion via urinary tract interferes with evaluation on ^{18}FDG-PET.(14,15) However, the role of ^{11}C-choline PET scan in the staging of bone and soft tissue sarcomas has not been clarified. To fully elucidate the role of ^{11}C-choline PET, the comparison with ^{18}FDG-PET and conventional imaging modalities are needed.

A new-modality PET/CT can improve the localization of tumors and accuracy of staging in patients because anatomic and molecular information can be coregistered precisely.(16) The aim of the current study was to compare the diagnostic accuracy between ^{11}C-choline PET/CT and conventional imaging for the staging of bone and soft tissue sarcomas.

Materials and Methods

Patient. We retrospectively reviewed ^{11}C-choline PET/CT results from September 2005 to March 2006 for patients with bone and soft tissue sarcomas, who subsequently underwent surgical resection, chemotherapy and/or radiotherapy within 2 weeks. ^{11}C-choline PET/CT was performed for initial staging in 12 patients and for restaging of recurrent disease in four patients. The study population consisted of 13 men and three women with a mean age of 44 years (range, 13–75 years). The clinical records of all of the patients were available for review. This study was conducted in accordance with the amended Helsinki declaration and the protocol was approved by the Institutional Review Board (National Cancer Center, Research Center for Cancer Prevention and Screening). All of the patients provided their written informed consent to participate in the present study and to review their records and images.

Radiopharmaceuticals. Carbon-11 choline was synthesized with a commercial module essentially using the method described by Hara and Yuasa.(17) $^{11}CO_2$ was converted to ^{11}C-methyl iodide by $LiAlH_4$/HI reaction. ^{11}C-methyl iodide was trapped in dimethylaminoethanol. After a washing step with ethanol and water, ^{11}C-choline retained on a cation exchange resin was eluted with saline. Radiochemical purity of the solution was evaluated by liquid chromatography radiodetector. The organic solvents were analyzed by gas chromatography. Endotoxin was assayed by the lysosomal acid lipase method.

PET/CT. Scans were acquired with a PET/CT device (Aquiduo; Toshiba Medical Systems, Tokyo, Japan) that consisted of a PET scanner (ECAT HR+; CTI, Knoxville, TN, USA) and 16-section CT scanner (Aquilion V-detector; Toshiba Medical Systems) with a whole-body mode implemented as the standard software. Prior to the ^{11}C-choline PET/CT study, the patients fasted for at least

[6]To whom correspondence should be addressed. E-mail: kuenstreli@nifty.com

doi: 10.1111/j.1349-7006.2006.00288.x

Table 1. Summary of patients and confirmed staging

Patient no.	Diagnosis	SUV	Size (mm)	Staging type	Location	TNM	Metastasis	Grade	Stage
1	Leiomyosarcoma	4.63	110	Initial	Retroperitoneum	T2bN0M1	Soft tissue	High	IV
2	Rhabdomyosarcoma	3.03	60	Initial	Perineum	T2bN1M0	Lymph node	High	IV
3	Pleomorphic malignant Fibrous histiocytoma	15.05	133	Initial	Chest wall	T2bN0M1	Bone, pleura, lymph node	High	IV
4	Leiomyosarcoma	4.10	80	Initial	Retroperitoneum	T2bN0M,P	Lung	Low	IV
5	Osteosarcoma	6.70	110	Initial	Iliac bone	T2N0M1b	Bone, lung	High	IVB
6	Clear cell sarcoma	13.03	80	Initial	Chest wall	T2bN0M1	Bone, lung, pleura, lymph node	High	IV
7	Myxoid liposarcoma	2.15	50	Initial	Leg	T1aN1M0	Lymph node	Low	IVB
8	Osteosarcoma	5.31	110	Initial	Tibia	T2N1M0	Lymph node	High	IV
9	Ewing sarcoma	3.46	95	Initial	Leg	T2bN0M0	N/A	High	III
10	Ewing sarcoma	9.86	102	Initial	Shoulder	T2N0M0	N/A	High	IIB
11	Ewing sarcoma	6.14	16	Initial	Spine	T1N0M0	N/A	High	IA
12	Chondrosarcoma	5.99	110	Initial	Iliac bone	T2N0M1b	Bone	High	IVB
13	Leiomyosarcoma	3.18	50	Restaging	Thigh	T1bN1M1	Bone, soft tissue, lymph node	High	IV
14	Osteosarcoma	4.95	75	Restaging	Jaw	T1N0M1a	Lung	High	IVA
15	Osteosarcoma	3.60	50	Restaging	Femur	T1N0M1b	Lung, bone	High	IVB
16	Alveolar soft part sarcoma	3.60	25	Restaging	Shoulder	T2N0M1	Bone	High	IV

N/A, not applicable; SUV, standardized uptake value; TNM, Tumor Node Metastasis.

6 h. CT was performed from the head to the mid-thigh according to a standardized protocol with the following setting: axial 3.0-mm collimation × 16 modes; 120 kVp; 100 mAs; and a 0.5-second tube rotation, pitch 11.0. Patients maintained normal shallow respiration during the three-dimensional acquisition of CT scans. No iodinated contrast material was administered. Emission scans from the base of the skull to the leg were obtained starting 5 min after the intravenous administration of 350–573 MBq of ^{11}C-choline. The acquisition time for PET was 2 min per table position. Images were reconstructed with attenuation-corrected ordered-subset expectation maximization with two iterations and eight subsets using emission scans and CT data.

Positron emission tomography, CT and coregistered PET/CT images were analyzed with dedicated software (e-soft; Siemens). The initial review of the attenuation-corrected PET images was performed using transaxial, coronal and sagittal planes. The images were reviewed and a consensus was reached by two board-certified radiologists who were unaware of any clinical or radiological information using a multimodality computer platform. ^{11}C-choline uptake was considered to be abnormal when it was substantially greater than the surrounding normal tissue. For ^{11}C-choline PET/CT, tumor sizes and T staging were determined by the CT part of PET/CT. ^{11}C-choline-avid lymph nodes or distant metastases on PET/CT were interpreted as positive for metastases regardless of size. Lymph nodes with abnormal uptake were deemed positive for metastases even when they were smaller than 10.0 mm in short axis nodal diameter. Lung nodules without abnormal uptake but highly suggestive of lung metastases on ^{11}C-choline PET/CT were considered to be positive for metastases. A pixel region of interest (ROI) was outlined within regions of increased ^{11}C-choline uptake and measured on each slice. For quantitative interpretations, standardized uptake value (SUV) was determined according to the standard formula, with activity in the ROI given in Bq per mL/injected dose in Bq per weight (kg). However, time decay correction for whole-body image acquisition was not conducted. A SUV of more than 2.5 was considered to characterize malignancy.

Conventional imaging. Conventional imaging methods, performed within 2 weeks of ^{11}C-choline PET/CT, either before or after, were ^{99,m}Tc-hydroxymethylene diphosphonate (HMDP) bone scintigraphy, chest CT and MRI of the primary site. ^{99,m}Tc-HMDP bone scintigraphy was performed 2 h after intravenous injection of 740 MBq of ^{99,m}Tc-HMDP. Both anterior and posterior whole-body planar images were obtained simultaneously with a dual-headed gamma camera (E.CAM; Siemens). Chest CT was performed using a multidetector scanner (Aquilion V-detector; Toshiba Medical Systems) with the following setting: axial 4.0-mm × 4 modes; 120 kVp, automated electric current; 0.5-second tube rotation; and pitch 5. Images were reconstructed with 10.0-mm slice thickness by means of a standard algorithm. MRI of the primary site was performed using a 1.5 Tesla system (Signa Horizon; GE Medical Systems, Milwaukee, WI, USA or Visart; MRI produced by Toshiba Medical Systems, Tokyo, Japan). Pulse sequences comprised T1-weighted spin echo (SE) images, T2-weighted fast spin echo (FSE) images, as well as post-contrast T1-weighted SE images with fat suppression after injection of contrast material. Pulse sequence parameters and slice orientation varied with the examined anatomic site. The images were reviewed and a consensus was reached by two board-certified radiologists who were unaware of any clinical or radiological information using hard-copy films and multimodality computer platform. The two readers for ^{11}C-choline PET/CT and those for conventional imaging were not the same persons.

Each tumor was staged according to the Tumor Node Metastasis (TNM) classification of the International Union Against Cancer for sarcoma of bone and the American Joint Committee staging protocol for sarcoma of the soft tissue.[18,19] T, N and M stages were assigned for both PET/CT and conventional imaging. T staging was confirmed by pathological evaluation using specimens obtained from surgical resection of the primary tumors. N staging was confirmed by pathological examinations in two patients using specimens obtained from sampling of regional nodes. In terms of extraregional nodes in two patients, nodal staging was confirmed by an obvious progression in number and/or size of the lesions on follow-up examinations. The mean follow-up period was 172 days (range, 44–322 days).

Statistical analysis. All valuables were assessed on a patient-by-patient basis. The McNemar test was used for paired comparisons between ^{11}C-choline PET/CT and conventional imaging. Statistical analysis was performed with the SPSS version 11 software program (SPSS, Chicago, IL, USA).

Results

There were eight bone sarcomas and eight soft tissue sarcomas (Table 1). The primary sites included shoulder ($n = 2$), chest wall

doi: 10.1111/j.1349-7006.2006.00288.x

Table 2. Staging of bone and soft tissue sarcoma

Variables	^{11}C-choline PET/CT	Conventional imaging	*P*-value
Overall stage			0.023
Correct	15 (94)	8 (50)	
Understaged	1 (6)	8 (50)	
Overstaged	0	0	
N stage			0.041
Correct	16 (100)	10 (63)	
Understaged	0	6 (38)	
Overstaged	0	0	
M stage			0.617
Correct	15 (94)	13 (81)	
Understaged	1 (6)	3 (19)	
Overstaged	0	0	

Note: Data are presented as number (*n*). Numbers in parentheses are percentages. CT, computed tomography; PET, positron emission tomography.

($n = 2$), retroperitoneum ($n = 2$), iliac bone ($n = 2$), leg ($n = 2$), thigh ($n = 1$), perineum ($n = 1$), tibia ($n = 1$), femur ($n = 1$), mandible ($n = 1$) and spine ($n = 1$). Pathological diagnoses were osteosarcoma ($n = 4$), Ewing sarcoma ($n = 3$), leiomyosarcoma ($n = 3$), clear cell sarcoma ($n = 1$), chondrosarcoma ($n = 1$), pleomorphic malignant fibrous histiocytoma ($n = 1$), myxoid liposarcoma ($n = 1$), rhabdomyosarcoma ($n = 1$), and alveolar soft part sarcoma ($n = 1$). Histological grade of tumors was grade 1 ($n = 1$), grade 2 ($n = 1$), grade 3 ($n = 11$) and grade 4 ($n = 3$).

All patients of initial staging had increased ^{11}C-choline uptake of the primary lesion (average maximal SUV ± SD: 5.92 ± 3.68 [range, 2.15–15.05]). Pathological T stages available in patients with initial staging are as follows: T1 ($n = 1$), T1a ($n = 1$), T1b ($n = 1$), T2 ($n = 4$) and T2b ($n = 5$). T stages in patients with restaging were T1 ($n = 2$), T1b ($n = 1$) and T2 ($n = 1$). Tumor size of patients for initial staging was 78.5 ± 34.0 mm (mean ± SD [range, 16.0–133.0 mm]). Both ^{11}C-choline PET/CT and conventional imaging classified the T stage correctly in all patients. Twelve (75%) of the 16 patients had N0 disease. Using ^{11}C-choline PET/CT, the N stage was correctly assigned in all patients, whereas the accuracy of conventional imaging in N stage was 63% ($P = 0.041$, Table 2). Understaging occurred in six patients (38%). Three of these patients (19%) had metastasis of inguinal node whose largest diameter was less than 10.0 mm (Fig. 1). The incidence of distant metastases was high in our study population. Both ^{11}C-choline PET/CT and conventional imaging detected bone metastases in seven patients (44%), lung metastases in five (31%) and pleural dissemination in two (18%, Fig. 2). Using ^{11}C-choline PET/CT, the M stage was correctly assigned in 15 patients (94%), whereas the accuracy of conventional imaging in M stage was 81% ($P = 0.617$, Table 2).

The complete stages of all patients were stage IA ($n = 1$), stage IIB ($n = 1$), stage III ($n = 1$) and stage IV ($n = 13$). TNM stage was correctly assessed with ^{11}C-choline PET/CT in 15 of 16 patients (94%) and with conventional imaging in eight of 16 patients (50%, $P = 0.023$, Table 2). ^{11}C-choline PET/CT assigned an incorrect TNM stage in a patient. This patient was understaged due to small metastatic lung tumor which was not clearly visualized by CT part of ^{11}C-choline PET/CT. Eight patients were understaged by conventional imaging (50%). Of these, skip metastases of soft tissues were identified in two (25%) and small nodal metastases in six (75%). ^{11}C-choline PET/CT correctly determined TNM stage in seven patients (44%) in whom stage derived from conventional imaging was incorrect.

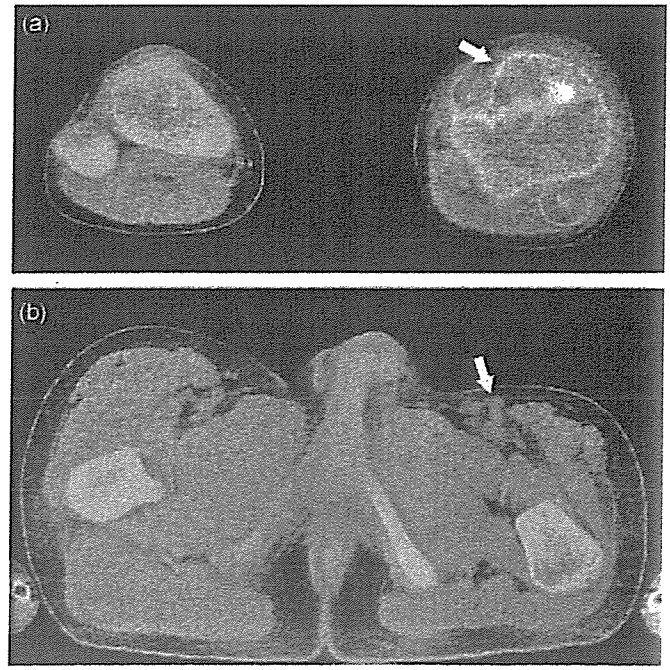

Fig. 1. A 13-year-old boy with osteosarcoma. (a) Transverse ^{11}C-choline positron emission tomography (PET)/computed tomography (CT) image revealed hypermetabolic focus in the proximal portion of the left tibia (arrow). PET/CT findings were verified at histopathological analysis. (b) Abnormal uptake of ^{11}C-choline was also noted in the left inguinal lymph node, which was interpreted as highly suspicious for malignancy (arrow). Subsequent resection revealed metastasis from osteosarcoma.

Discussion

The results of the present study show that ^{11}C-choline PET/CT improves the accuracy of staging in patients with bone and soft tissue sarcomas compared to conventional imaging. Specifically, ^{11}C-choline PET/CT has potentially significant implications for detecting nodal and distant metastases at overall staging. Reports about the efficacy of ^{11}C-choline in the localization and detection of bone and soft tissue sarcomas are still limited.[15] To our knowledge, no study regarding ^{11}C-choline PET/CT for staging bone and soft tissue sarcomas was found. In our study, seven of the 16 patients had skip metastases of soft tissue or nodal metastases detected by ^{11}C-choline PET/CT that were not identified by routine clinical and conventional radiological evaluation.

The ability of PET to depict increased metabolism in malignancies has greatly improved the accuracy in detecting neoplasms.[4] However, compared with conventional imaging studies, use of PET alone results in a lack of substantial detail.[20] The PET/CT device permits sequential acquisition of anatomic CT and functional PET images in a single scanning session. Morphological characterization of scintigraphic lesions by PET/CT resulted in a lower percentage of equivocal interpretations compared with that of conventional imaging. Tumor-detecting PET/CT technology is growing rapidly. However, there are only limited data available on staging of bone and soft tissue sarcomas with PET/CT.

Carbon-11 choline uptake was significantly higher in malignant soft tissue tumors and was due to the high utilization of cell membranes of these lesions. ^{11}C-choline uptake is observed physiologically in the liver, pancreas, kidney and duodenum. ^{11}C-choline is also secreted into phospholipid-rich pancreatic juice in a non-fasting state. A potential advantage of ^{11}C-choline PET/CT might be the assessment of tumors in the skull or retroperitoneum. Blood clearance of ^{11}C-choline is rapid and radioactive distribution

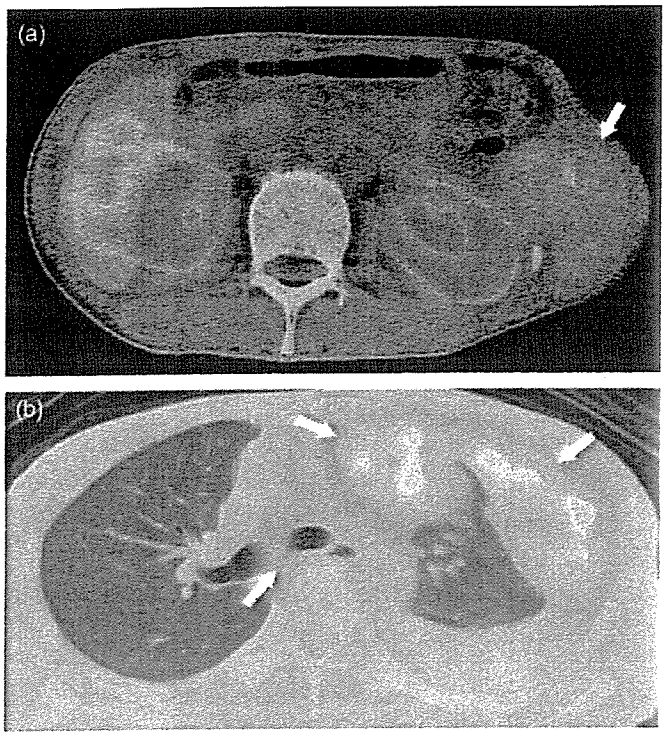

Fig. 2. A 34-year-old man with clear cell sarcoma. (a) Transverse ^{11}C-choline positron emission tomography (PET)/computed tomography (CT) image depicting abnormal uptake in the tumor arising from the left lateral chest wall (arrow). (b) PET/CT image also depicts pleural dissemination and mediastinal lymph node (arrows). Follow-up findings in this patient confirmed the diagnosis.

in tissues is constant in 5 min. The accumulation of ^{11}C-choline in the skull or retroperitoneum is hardly affected by background within the limits of short uptake time. In comparison to ^{18}FDG, physiological background level in the urinary tract is low. This may be due to incomplete tubular reabsorption of the intact tracer, or enhanced excretion of labeled oxidative metabolites like betaine.[12]

Limited resolution of the present generation of ^{11}C-choline PET/CT and the partial volume effect result in failure to detect small lesions. In our study, one patient was understaged due to small metastatic lung tumor, which was not visualized clearly by the CT part of ^{11}C-choline PET/CT. Faint increase in tracer uptake and motion artifact caused by breathing contribute to false negative results. However, the advantage of ^{11}C-choline PET/CT is that the whole-body can be visualized in a single examination. In our study, 50% of patients were understaged by conventional imaging. The inaccuracy of conventional imaging in assessing skip metastases of soft tissues is due to the field of view.

We reported the accurate modality of ^{11}C-choline PET/CT as a non-invasive method for staging in patients with bone and soft tissue sarcomas compared to conventional imaging. Choline is an essential component of the cell membrane, and choline uptake may be via a choline-specific transporter protein. Choline kinase, which catalyzes the phosphorylation of choline, is upregulated in tumor cells.[12] In some types of tumor cells, overexpression of choline-specific transporter protein and choline kinase were identified by *in situ* hybridization.[21] ^{11}C-choline will be phosphorylated by choline kinase as a choline analog and retained in tumor cells.[21] However, the precise pathway of metabolic trapping by tumor cells has not been elucidated, and further studies to clarify the mechanism of imaging by ^{11}C-choline are needed.

Our study has limitations. Most patients in this study had high-grade tumors (88%) and may differ from the patient population of previous studies. Our study was intended to examine the staging prior to treatment; therefore, patient population of high-grade tumors may explain the significant accuracy in overall staging compared to conventional imaging. A study with a larger patient population would clarify the influence of ^{11}C-choline PET/CT on staging. ^{11}C-choline is clearly a sensitive PET tracer for staging patients with bone and soft tissue sarcomas. The short half-life of ^{11}C-choline necessitates the availability of an on-site cyclotron, which causes practical restriction. More specific radiotracers will help overcome this limitation in the future.

In summary, the use of ^{11}C-choline PET/CT in patients with bone and soft tissue sarcomas increases the accuracy of overall staging and N staging compared to conventional staging. Our study suggests that whole-body ^{11}C-choline PET/CT should be the preferred modality for staging in patients with bone and soft tissue sarcomas.

References

1 Reuther G, Mutschler W. Detection of local recurrent disease in musculoskeletal tumors: magnetic resonance imaging versus computed tomography. *Skeletal Radiol* 1990; **19**: 85–90.
2 Nieweg OE, Pruim J, van Ginkel RJ *et al.* Fluorine-18-fluorodeoxyglucose PET imaging of soft-tissue sarcoma. *J Nucl Med* 1996; **37**: 257–61.
3 Eary JF, Conrad EU, Bruckner JD, Folpe A, Hunt KJ, Mankoff DA, Howlett AT. Quantitative [F-18]fluorodeoxyglucose positron emission tomography in pretreatment and grading of sarcoma. *Clin Cancer Res* 1998; **4**: 1215–20.
4 Franzius C, Sciuk J, Daldrup-Link HE *et al.* FDG-PET for detection of osseous metastases from malignant primary bone tumors: comparison with bone scintigraphy. *Eur J Nucl Med* 2000; **27**: 1305–11.
5 Schwarzbach MHM, Dimitrakopoulou-Strauss A, Willeke F *et al.* Clinical value of [18-F]fluorodeoxyglucose positron emission tomography imaging in soft tissue sarcomas. *Ann Surg* 2000; **231**: 380–6.
6 Ioannidis JP, Lau J. 18F-FDG PET for the diagnosis of soft-tissue sarcoma: a meta-analysis. *J Nucl Med* 2003; **44**: 717–24.
7 Tateishi U, Yamaguchi U, Seki K *et al.* Glut-1 expression and enhanced glucose metabolism are associated with tumor grade in bone and soft tissue sarcomas: a prospective evaluation by [F-18]-fluorodeoxyglucose positoron emission tomography. *Eur J Nucl Med Mol Imaging* 2006; **33**: 683–91.
8 Hara T, Kosaka N, Shinoura N *et al.* PET imaging of brain tumor with [methyl-^{11}C]choline. *J Nucl Med* 1997; **38**: 842–7.
9 Hara T, Kosaka N, Kishi H. PET imaging of prostate cancer using carbon-11-choline. *J Nucl Med* 1998; **39**: 990–5.
10 Hara T, Inagaki K, Kosaka N *et al.* Sensitive detection of mediastinal lymph node metastasis of lung cancer with ^{11}C-choline PET. *J Nucl Med* 2000; **41**: 1507–13.
11 Torizuka T, Kanno T, Futatsubashi M *et al.* Imaging of gynecologic tumors: comparison of ^{11}C-choline PET with ^{18}F-FDG PET. *J Nucl Med* 2003; **44**: 1051–6.
12 Ishidate K. Choline/ethanolamine kinase from mammalian tissues. *Biochim Biophys Acta* 1997; **1348**: 70–8.
13 Maeda T, Tateishi U, Komiyama M *et al.* Distant metastasis of prostate cancer: Early detection of recurrent tumor with dual-phase carbon-11 choline positron emission tomography/computed tomography in two cases. *Jpn J Clin Oncol* in press.
14 Zhang H, Tian M, Oriuchi N *et al.* ^{11}C-choline PET for the detection of bone and soft tissue tumours in comparison with FDG PET. *Nucl Med Commun* 2003; **24**: 273–9.
15 Tian M, Zhang H, Oriuchi N *et al.* Comparison of ^{11}C-choline PET and FDG PET for the differential diagnosis of malignant tumors. *Eur J Nucl Med Mol Imaging* 2004; **31**: 1064–72.
16 Bar-Shalom R, Yefremov N, Guralnik L *et al.* Clinical performance of PET/CT in evaluation of cancer: additional value for diagnostic imaging and patient management. *J Nucl Med* 2003; **44**: 1200–9.
17 Hara T, Yuasa M. Automated synthesis of [^{11}C]choline, a positron-emitting tracer for tumor imaging. *Appl radiat Isot* 1999; **50**: 531–3.
18 Green FL, Page DL, Fleming ID *et al. AJCC Cancer Staging Manual*, 6th edn. New York: Springer, 2002.
19 Sobin LH, Wittekind C. *UICC TNM Classification of Malignant Tumours*, 6th edn. New York: Wiley, 2002.
20 Franzius C, Daldrup-Link HE, Wagner-Bohn A *et al.* FDG-PET for detection of recurrences from malignant primary bone tumors: comparison with conventional imaging. *Ann Oncol* 2002; **13**: 157–60.
21 Uchida T, Yamashita S. Molecular cloning, characterization, and expression in *Escherichia coli* of a cDNA encoding mammalian choline kinase. *J Biol Chem* 1992; **267**: 10 156–62.

doi: 10.1111/j.1349-7006.2006.00288.x

Local Delivery of Doxorubicin for Malignant Glioma by a Biodegradable PLGA Polymer Sheet

YOSHINOBU MANOME[1], TOSHIAKI KOBAYASHI[2], MARIKO MORI[3], RIE SUZUKI[1], NAOTAKE FUNAMIZU[1], NOBUTAKE AKIYAMA[4], SACHIKO INOUE[5], YASUHIKO TABATA[5] and MICHIKO WATANABE[1]

Departments of [1]Molecular Cell Biology, [3]Pathology and [4]Molecular Immunology, Jikei University School of Medicine, 3-25-8 Nishishinbashi, Minato-ku, Tokyo, 105-8461; [2]Cancer Screening Technology Division, Research Center for Cancer Prevention and Screening, National Cancer Center, 5-1-1 Tsukiji, Chuo-ku, Tokyo, 105-0045; [5]Department of Biomaterials, Institute for Frontier Medical Sciences, Kyoto University, 53 Kawara-cho Shogoin, Sakyo-ku, Kyoto 606-8507, Japan

Abstract. *Implantable, biocompatible and biodegradable devices bearing an anticancer drug can provide promising local therapy to patients with malignant disorders. With the aim of treating brain tumors, especially gliomas, a membranous sheet containing doxorubicin was produced by co-polymerization to poly(D,L-lactide-co-glycolide) (PLGA). When release of the drug from the sheet was measured, sustained release continued until day 34. The data contrasted with the burst release from material containing a higher proportion of the drug. In terms of biodegradability, a subcutaneous 3 x 3-mm tetragonal sheet was almost completely absorbed by day 80. When a glioma was implanted subcuteneously and the tumor nodule exposed to the sheet, the device inhibited tumor growth significantly. The sheet consisted of an amorphous structure with cavities estimated to have a diameter of 0.5 – 3 μm by electron microscopic observation. Since the sheet is implantable, biodegradable and has a sustained-drug release property, the device may play a role in the local therapy of brain tumors.*

Malignant brain tumor, such as infiltrating glioma and glioblastoma, is one of the most intractable diseases in the human body. The invasive character and rapid proliferation of the cells often brings recurrence of the disease even after radical treatment and an increase in intracranial hypertension eventually causes herniation due to limited intracranial space. The median survival time is 0.4 years for glioblastoma and is 5.6 years even for more benign low-grade astrocytoma (1). Most patients die within 2 to 5 years after their diagnosis. In spite of recent advances in radiotherapy, immunotherapy, chemotherapy and other adjuvant therapies, the prognosis has not been dramatically improved and more effective therapies are required. Although the prognosis is poor, the tumors seldom metastasize to regions outside of the central nervous system. In addition, the main etiology of death is local recurrence. Therefore, if local recurrence can be prevented, long-term survival or even a complete cure of the patient can be expected.

The main problem of administering chemotherapy for malignancy in the central nervous system is the low efficiency of drug delivery to the residual tumor in brain parenchyma. When anti-malignant drugs are systemically administered, most drugs may not reach the lesion due mainly to the existence of the blood-brain barrier. From the aspect of chemotherapy, alkylating agents such as temozolomide and nitrosourea represented by ACNU or BCNU are the first choice of drugs in combination with radiation (2, 3). These drugs are potent against malignant gliomas since they can cross the blood-brain barrier and enter the tumor cells. They confer toxicity even to not-actively dividing cells, which account for approximately 70% of the brain tumor (4). Moreover, alkylating agents can synchronize cells in the G2M phase and, thus, function as radiosensitizers when combined with therapeutic irradiation. Regardless of such a promising efficacy of the drug, the prognosis of patients has not improved sufficiently. The reason is partly attributable to the low local drug concentration, because the drug delivery is not adequate in spite of penetrability of the drug through the blood-brain barrier (5, 6). When these facts are considered, it is obvious that the development of more potent local treatment is required.

Correspondence to: Yoshinobu Manome, MD, Ph.D., Department of Molecular Cell Biology, Institute of DNA Medicine, Jikei University School of Medicine, Japan. Tel: +81-3-3433-1111 Ext. 2360, Fax: +81-45-628-4757, e-mail: manome@jikei.ac.jp

Key Words: Doxorubicin, PLGA, local delivery, glioma.

Recent advances in material engineering have provided a new material for such local treatment. One representative example is the BCNU-loaded PLGA wafer (7). PLGA is a biodegradable and biocompatible material, and the BCNU-loaded PLGA wafer is an implantable polymeric device that releases BCNU directly into the tumor tissue. Implanting the device after surgery can eliminate the residual tumor tissue in the operative field and delay recurrence. The antitumor activity of the wafer has been demonstrated (8, 9) and the device might be useful because most patients with glioma undergo surgical removal and chemotherapy as well as radiotherapy.

However, there is a concern about alkylating agent-based local chemotherapy, because tumor cells soon acquire resistance after the systemic administration of drugs. The mechanism of resistance is mainly *via* the recruitment of O_6-methylguanin merthyltransferase, a DNA repair enzyme into tumor cells (10-13). MGMT facilitates stoichiometric transfer of the O_6-alkyl groups from the alkylated DNA molecules to its own cysteine residues and by so doing, is itself deactivated after acceptance of the alkyl groups. Overexpression of MGMT repairs the DNA damage caused by the alkylating agents. Chemotherapeutic agents, such as temozolomide and nitrosourea, induce MGMT expression in the tumor cells and resistance may influence the effect of focal treatment with the BCNU wafer. In such cases, treatment with another anti-malignant drug with a different mechanism of action might be useful. Based on this concept doxorubicin was selected.

The mechanism of doxorubicin resistance is expression of the multiple drug resistant gene (MDR); moreover, it does not show cross-resistance to alkylating agents. In addition, doxorubicin has been used commonly in patients with disseminated lymphoma or leukemia in the cerebrospinal fluid by intrathecal injection and its safety has been well recognized. Thus, doxorubicin was co-polymerized to biodegradable PLGA and a membrane containing the drug was developed. Ultimately, the possibility of modulating the glioma after surgery using the membrane could be explored.

Materials and Methods

Doxorubicin sheet. Doxorubicin hydrochloride ((2S,4S)-4-(3-amino-2,3,6-trideoxy-α-L-*lyxo*-hexopyranosyloxy)-1,2,3,4-tetrahydro-2,5,12-trihydroxy-2-hydroxyacetyl-7-methoxynaphthacene-6,11-dione monohydrochloride; DOX or Adriamycin) was provided by Kyowa Hakko Kogyo Co. Ltd. (Tokyo, Japan). One square centimeter of the sheet contained 1 mg of doxorubicin. To prepare an 8.4 cm^2 surface of the sheet, 8.4 mg of doxorubicin were mixed with 318 mg of PLGA (50:50 molar ratio, Mw53114) dissolved in chloroform. The mixture was co-polymerized by the solvent-evaporation method and used after further desiccation.

Release of doxorubicin in vitro. Measurement of the drug concentration in the solvent was determined by the UV-2200A spectrophotometer (Shimadzu, Kyoto, Japan). The doxorubicin sheet was set under physiological conditions for days (pH7.4, 37°C in phosphate-buffered saline) and the total amount of the eluted doxorubicin was quantified.

Animal experiments. To investigate the biodegradation of the doxorubicin sheet, closed colony Jcl:ICR mice were purchased from Clea Japan, Tokyo and bred in a standard animal facility. For the tumor implantation and treatment study, five-week old Fischer 344 rats were purchased from Sankyo Laboratory, Tokyo, Japan. These animals were maintained under conditions of 28°C and 55-60% humidity and given free access to food and tap water. All the animal procedures were performed under the guidance of the committee in the animal care facility. In the first set of animal experiments, the 3 x 3 mm tetragon sheet was subcutaneously implanted into the left flank of an ICR mouse. After implantation, absorption of the sheet was determined by weighing the unabsorbed residuals after removal. Degradability was expressed as a percentile of the original sheet weight on the day of observation (n=5 in each group). In the second set of the experiment, the RT2 glioma cell line, syngeneic to the Fischer 344 rat, was used. The RT2 glioma cells were cultured in Dulbecco's minimum essential medium supplemented with 10% bovine serum (GIBCO Laboratories, Grand Island, NY, USA). Three x 10^5 of the trypsinized and dispersed cells in 100 μl of PBS were subcutaneously injected into the rat's right flank and four days later, after confirmation of establishment of the tumor nodule, the rats were treated with 2.1125 cm^2 of doxorubicin sheet containing 2.1 mg of doxorubicin by covering the tumor. For some animals, 8.4 mg/100 μl of doxorubicin were directly injected into the center of the tumor. Tumor volumes were measured and growth was directly accessed. Statistical analysis was performed by the two-tailed Student's *t*-test.

Morphological examination of the doxorubicin sheet by electron microscopy. For the scanning electron microscopy, the doxorubicin sheet was lightly washed in water then fixed with 1.2% glutaraldehyde in 0.1 M phospate-buffered saline then adjusted to pH 7.4. The specimen was dehydrated by ascending concentrations of ethanol and the critical point drying method using liquid CO_2. After the dehydration, the sample was coated with ion-sputtered gold and palladium and observed by a JSM-5800LV Scanning Electron Microscope (JEOL Ltd., Tokyo, Japan) at the accelerating voltage of 15 KV. For transmission electron microscopy, the sheet was fixed with 2% glutaraldehyde in phosphate-buffer and the specimens were subjected to examination by an H-7500 Electron Microscope (Hitachi, Tokyo, Japan) at the accelerating voltage of 100 KV.

Results

Release of doxorubicin from the doxorubicin sheet. The release of doxorubicin from the PLGA membrane was first determined *in vitro*. The concentration of doxorubicin was measured by absorption spectrophotometric analysis. The absorbance of light by doxorubicin in continuous wavelength was measured by a spectrophotometer (Figure 1A) and the correlation of both 232 nm and 480 nm peaks for determination of the doxorubicin concentration was confirmed. The amount of drug in the solvent was

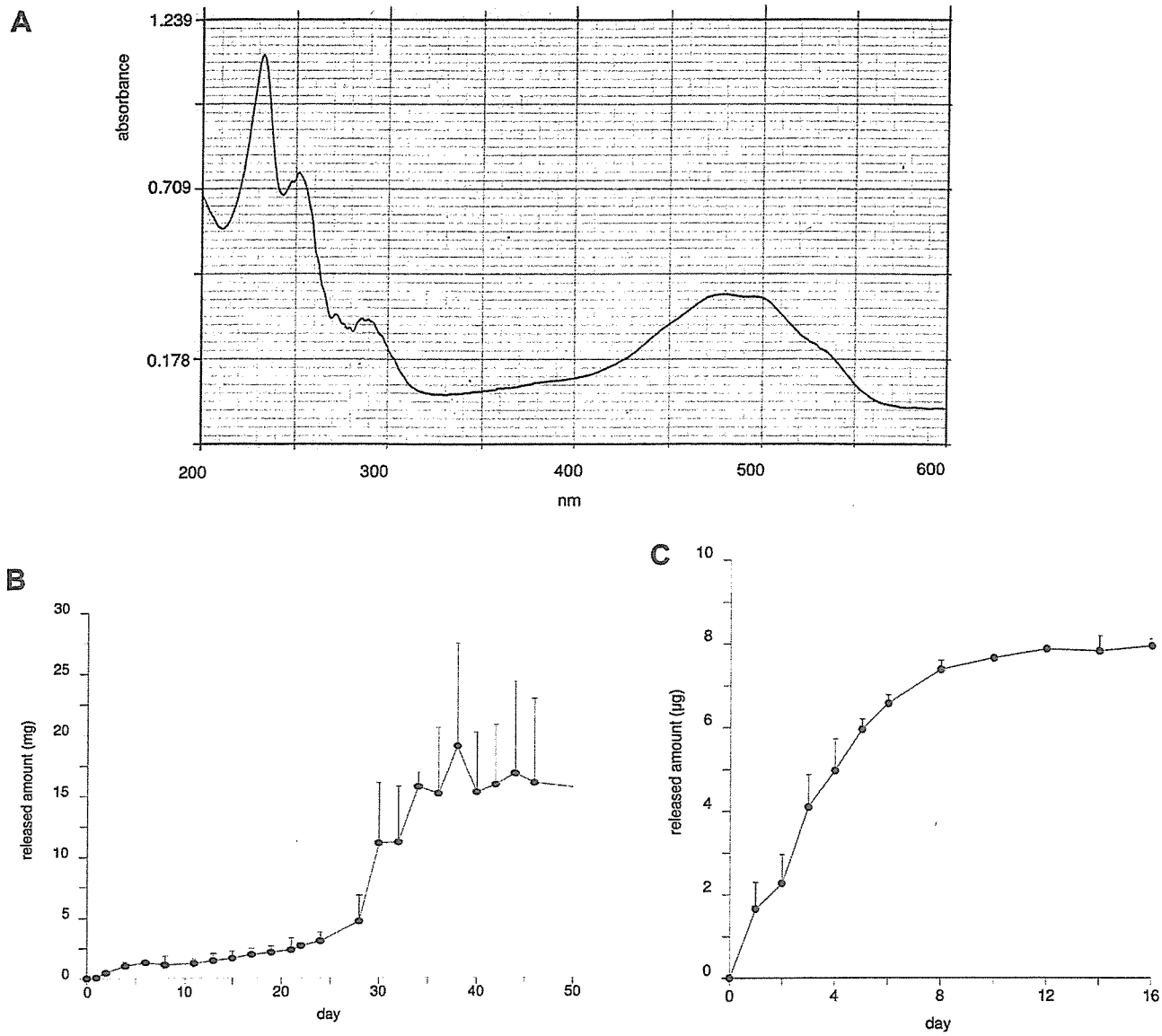

Figure 1. *Release of doxorubicin from the sheet in vitro. A) Spectrophotometric properties of doxorubicin. The light absorbance of doxorubicin was measured by continuous change in the wave length. Based on the figure, the absorbances at 232 nm and 480 nm were used for further determination of the drug concentration. Values measured at both peaks correlated well with drug concentrations. B) Total amount of doxorubicin released from 1 mg of the sheet. Release gradually started from immediately after the exposure and 10% of the drug was released by day 10. The sheet steadily discharged the drug and sustained release continued until day 28. After the burst release around day 30 to 34, further release was not detected. The result is expressed as the mean of two experiments; bars, S.D. C) Release from the drug-overloaded sheet. When the drug concentration was increased 3-fold when co-polymerized to PLGA, the sheet released the drug much faster than the ordinary sheet. Most of the drug was released by day 8 and further release was not prominent after day 10. The result is expressed as the mean of two experiments; bars, S.D.*

quantified at the 480-nm wavelength. The PLGA sheet containing doxorubicin was left under physiological conditions and the total amounts of doxorubicin released were measured (Figure 1B). Release started from day 1 and gradually increased until day 24. Subsequently, the release was abruptly increased and continued until day 34. Thirty-four days after the experiment, the release reached a peak. The released amount was followed up until day 178, however further release was not detected in the experiment (data not shown). The pattern of slow release from the sheet might derive from the proportions of doxorubicin and PLGA. When the load of doxorubicin was increased in the sheet, a three-fold higher drug discharge occurred at an earlier stage of the experiment (Figure 1C). The drug burst

started from the day of the experiment and most of the doxorubicin was released by day 8. Unlike the previous result, sustained release was not detected in this drug-enriched sheet. The sheet did not retain doxorubicin after 12 days of experiments.

Biodegradation of the sheet in mice. Since deliberate release of the drug from the sheet was demonstrated *in vitro*, the biodegradability of the sheet was examined next. After implantation of the sheet into the left flank of the mice, changes in the dry-weight of the sheet were measured and recorded chronologically. The sheet degraded according to the passage of time. Degradation rapidly progressed in the initial stage and continued until day 78. The sheet was ultimately absorbed. It took more than 80 days to disappear and further changes in weight could not be determined. During the process, the doxorubicin sheet was assimilated and other than pigmentation in the adjacent area, caused

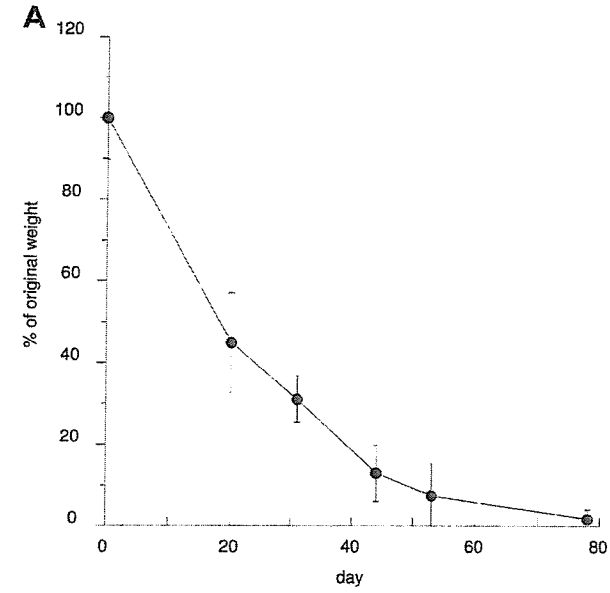

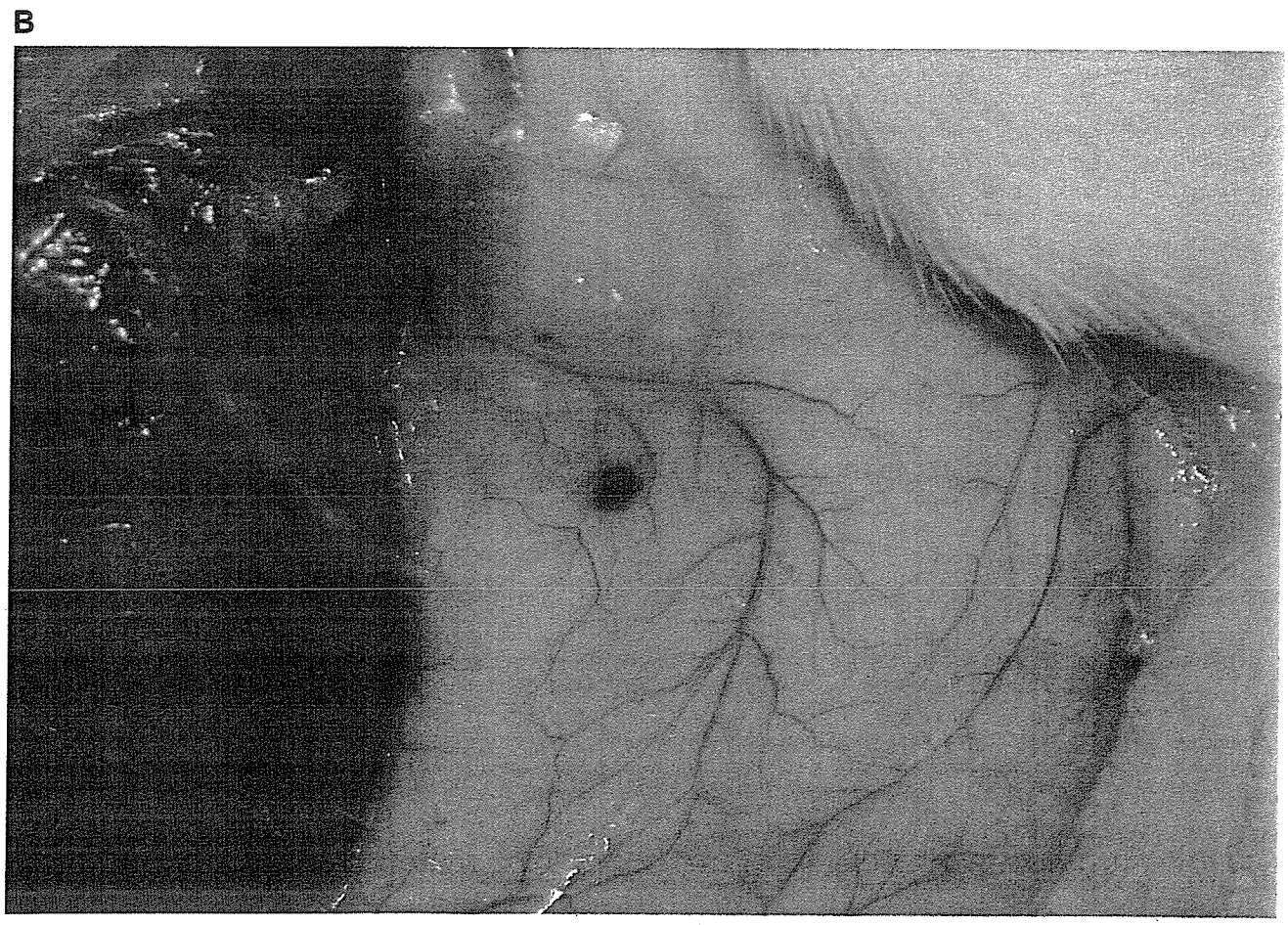

Figure 2. *Biodegradability of the sheet in vivo. A) The dry-weight of the implanted sheet was measured and biodegradability was expressed as a percentage of the original weight. The sheet degraded according to the passage of time. There was a rapid decrease in volume from the start of the experiment, followed by gradual degradation. More than 78 days were required for complete absorption. The result is expressed as the mean of five animals at each time point; bars, S.D. B) Biodegradability of the subcutaneously implanted sheet. The picture shows the sheets at 52 days after implantation. The sheet was degraded, but still visible with a change in the color of the surrounding subcutaneous tissue. Pigmentation of tissue occurred in the contact area of the sheet.*

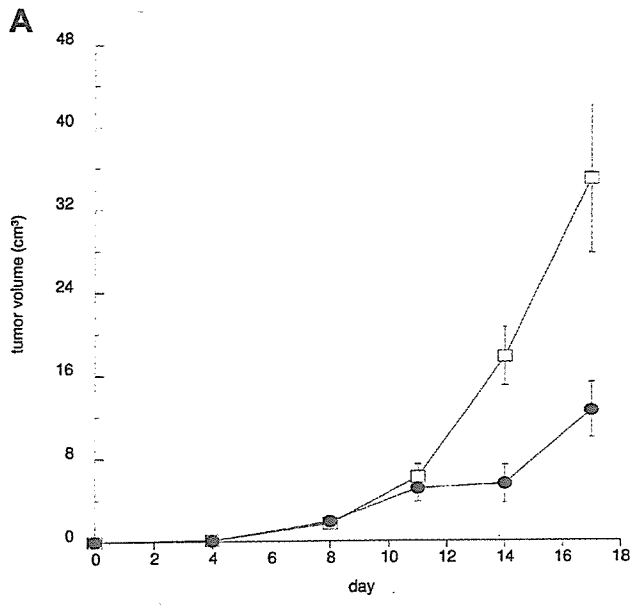

neither inflammation nor substantial necrosis in the surrounding tissue (Figure 2A, B).

Effect of the released doxorubicin on the established tumor. The slow-release character and biodegradability of the sheet enables potential application of the sheet for tumor treatment *in vivo*. In the final examination, the sheet was used for the treatment of subcutaneously implanted RT2 syngeneic malignant glioma tumor cells. After growth, the tumor was covered with a doxorubicin sheet and the subsequent growth was measured. Tumors treated with a mock sheet increased in size exponentially (Figure 3). In contrast, growth of the tumor was inhibited in rats treated with the doxorubicin sheet. On the 17th day of the experiment, the tumor volume reached more than 30 cm^3 and the rats started to die in the control group, whereas the group treated with the doxorubicin sheet exhibited a smaller tumor size. There were inter-group differences in volumes

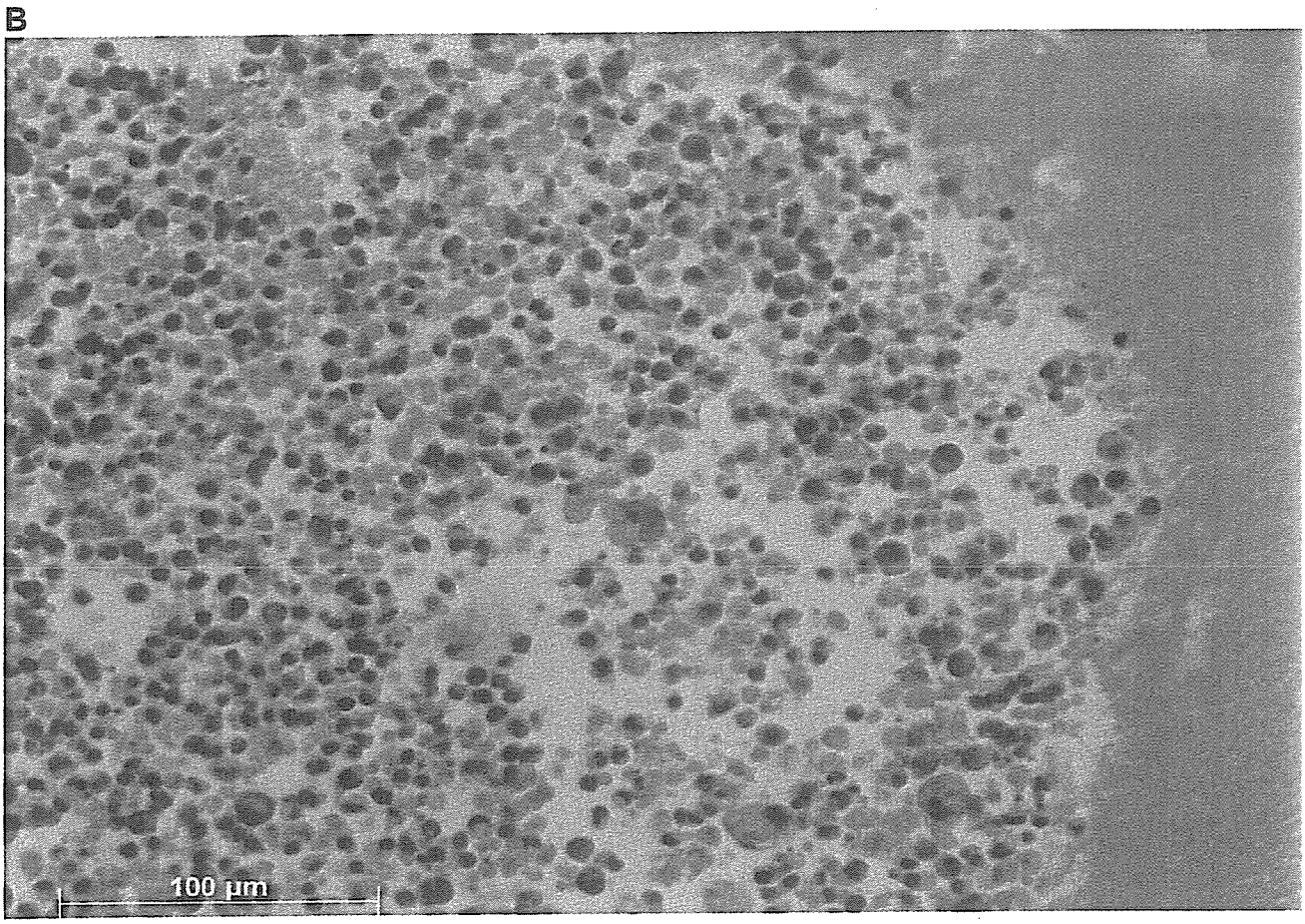

Figure 3. *Tumor growth inhibition by the sheet. A) After glioma cells were implanted, the tumor nodule was treated to the sheet. While tumors in control animals grew prosperously, treatment inhibited the expansion of the tumor. Mock sheet treatment (□); doxorubicin sheet treatment (●). There were differences on day 14 (p=0.064) and day 17 (p=0.019). The result was demonstrated as a mean of five animals in each group; bars, S.D. B) Histology of tumor cells with the sheet (on day 17, hematoxylin-eosin staining). Tumor tissue or cells (left) adjoining the sheet (right) were necrotic with erythrocytes.*

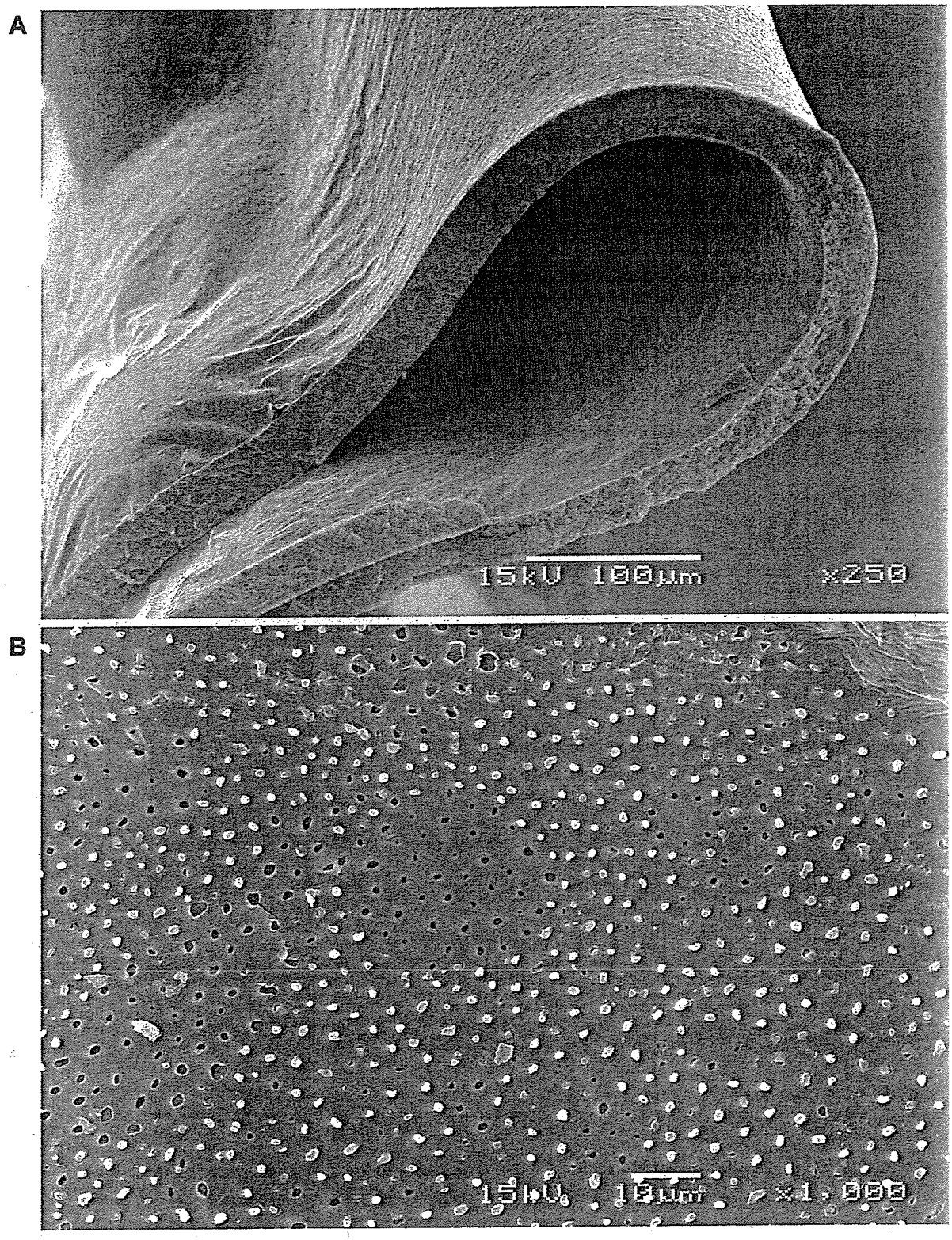

Figure 4. *Ultrastructure of doxorubicin sheet by electron microscopy. A-C) Pictures taken by scanning electron microscope, D) By transmission electron microscope. A) Overview: the sheet had a flexible texture with a thickness of 10 µm. B) Surface: the surface consisted of amorphous material with small holes. Grains of the drug resided in these small holes with a diameter of 0.5 to 3 µm. C) Vertical section (ethanol-cracked surface): after fixation, the sample was ethanol-cracked in liquid nitrogen. Cross-section disclosed the porous structure of the membrane sheet. D) Cross-section of the sheet: the drug was encircled by an amorphous electro-density substrate. Direct magnification, x15000.*

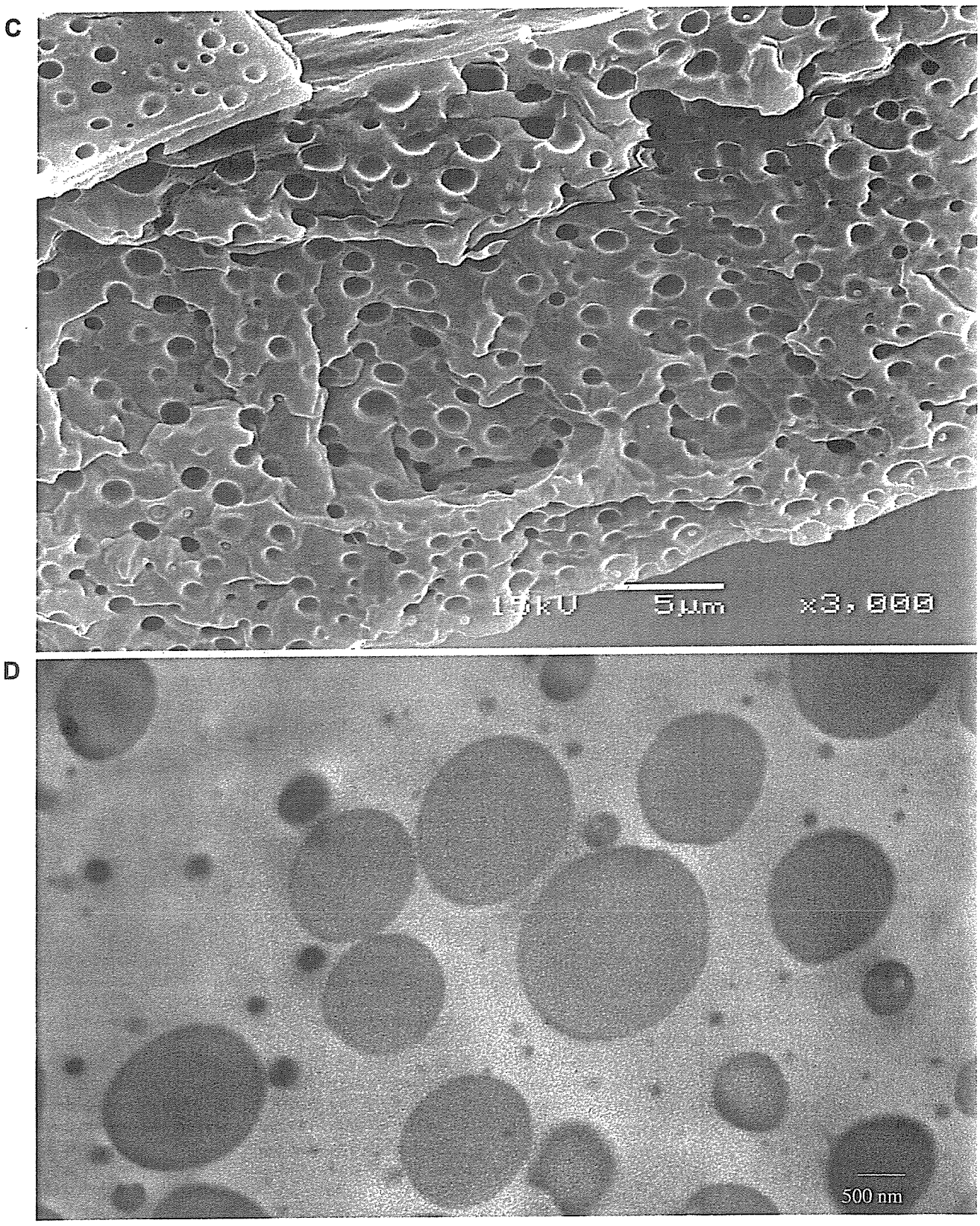

Figure 4. *continued*

on days 14 and 17 (p=0.064 and 0.019, respectively). The sizes of tumors treated with the doxorubicin sheet were comparable to those of animals treated by direct injection with a 4-times higher total dose (on day 14: injection 4.88±2.33 cm^3 *vs.* sheet 5.50±1.81 cm^3, on day 17: 14.80±6.62 cm^3 *vs.* 12.56±2.65 cm^3).

Morphological studies of the sheet. The sheet's ability to confer toxicity to the target tumor by releasing the drug was confirmed. To further investigate the material, the sheet was examined by electronmicroscopy. The sheet had a thickness of 10 μm and was flexible (Figure 4A). The surface of the sheet consisted of an amorphous structure with small cavities having a diameter of 0.5 to 3 μm. A grain, presumably of drug, was held in each cavity and some of these protruded to the surface. Some of the cavities were empty, but this may have been due to elution of the drug during preparation of the specimen (Figure 4B). An ethanol-cracked, vertical section revealed the spongy, cheese-like structure of the sheet. Most of the cavity was hollow due to the same reason as above, but the drug is visible in the cavities through a small exit (Figure 4C). This finding was confirmed by transmission electronmicroscopy (Figure 4D). The structure of the sheet may be responsible for sustained release of the drug.

Discussion

In this study, a doxorubicin-loaded poly (D, L-lactide-co-glycolide) membrane was developed and drug release from the membrane, biodegradation and efficacy on implanted glioma cells were examined.

As a scaffold for drug polymerization, PLGA was chosen. Similar to other polymers (14), PLGA has been used, not only as biodegradable polyester elastomers in tissue engineering (15), but also as a carrier of drugs, antigens, or genes either by itself or in combination with other appropriate materials. Owing to its safety, performance, cost and ease-of-use, this material was especially useful as a drug delivery tool for anticancer drugs. Micro- or nano-particles of PLGA conjugates include paclitaxel (16-20), doxorubicin (21-23), floxuridine (24), cystatins (25), camptothetin (26), 5-fluorouracil (27, 28), oxaliplatin (29), methotrexate (30) and cisplatin (31). In addition to the anticancer agents, tumor antigen (32, 33), photodynamic (34-37) or radiosensitizer (38, 39), genes (40-42) or DNA decoys (43), anti-angiogenic agents (44, 45), usnic acid (46), interferons (47), immunotoxin (48), all-trans retinoic acid (49), hormones (42, 50) and other compounds have been conjugated to PLGA for the treatment of malignant diseases.

Nano- or micro-particles of PLGA have drug delivery advantages, such as achievement of a higher concentration in the target tissue, sustained release and a longer circulation time in plasma as well as lower toxicity. However, from the stand-point of brain tumor therapy, especially considering the prevention of recurrence, there is an advantage of local therapy with an implantable drug-conjugated device, even though diffusion of nanoparticles is relatively limited to the vicinity of the implantation site (27). Accordingly, a wafer with BCNU was successfully developed (7, 8, 51). In other solid tumors, local treatment with PLGA polymers with paclitaxel and vinca alkaloid were developed and tested in clinical pilot trials (52, 53).

We chose doxorubicin for co-polymerization to PLGA. This drug has a long history and has been used widely for the treatment of malignancies, including leukemias, lymphomas and many solid tumors, including brain tumors. Accordingly, its pharmacokinetics are well known. From the aspect of safety, the drug can be administrated intrathecally with few serious adverse effects (54, 55). This might compromise safety if leakage of the drug occurs into the cerebrospinal fluid. Moreover, resistance to alkylating agent due mainly to overexpression of MGMT generally does not demonstrate cross-resistance to doxorubicin, which blocks DNA and RNA synthesis by inhibiting topoisomerase II. The sheet might be especially useful for patients with recurrent drug-resistant gliomas initially treated by alkylating agents.

Local therapies are key options for the treatment of brain tumors. BCNU-loaded wafers and other implantable nano- and micro-particles are the materials of first choice. It is preferable to increase the number of effective devices or drugs for local treatment. Since our PLGA-based sheet is implantable, easy to prepare, wholly degradable and displays a sustained-release property, it may play a role in the treatment for malignant brain tumors as a local therapy device.

Acknowledgements

The work was partly supported by a Grant-in-Aid for the Third Term Comprehensive Control Research for Cancer. We thank Hideki Saito, Emi Kikuchi and Yuko Abe in the Jikei University School of Medicine, Japan, for skillful technical assistances.

References

1 Ohgaki H and Kleihues P: Population-based studies on incidence, survival rates, and genetic alterations in astrocytic and oligodendroglial gliomas. J Neuropathol Exp Neurol *64*: 479-489, 2005.

2 Barrie M, Couprie C, Dufour H, Figarella-Branger D, Muracciole X, Hoang-Xuan K, Braguer D, Martin PM, Peragut JC, Grisoli F and Chinot O: Temozolomide in combination with BCNU before and after radiotherapy in patients with inoperable newly diagnosed glioblastoma multiforme. Ann Oncol *16*: 1177-1184, 2005.

3 Cohen MH, Johnson JR and Pazdur R: Food and Drug Administration Drug approval summary: temozolomide plus radiation therapy for the treatment of newly diagnosed glioblastoma multiforme. Clin Cancer Res *11*: 6767-6771, 2005.

4 Yoshii Y, Maki Y, Tsuboi K, Tomono Y, Nakagawa K and Hoshino T: Estimation of growth fraction with bromodeoxyuridine in human central nervous system tumors. J Neurosurg *65*: 659-663, 1986.

5 Hamstra DA, Moffat BA, Hall DE, Young JM, Desmond TJ, Carter J, Pietronigro D, Frey KA, Rehemtulla A and Ross BD: Intratumoral injection of BCNU in ethanol (DTI-015) results in enhanced delivery to tumor – a pharmacokinetic study. J Neurooncol *73*: 225-238, 2005.

6 Yimam MA, Bui T and Ho RJ: Effects of lipid association on lomustine (CCNU) administered intracerebrally to syngeneic 36B-10 rat brain tumors. Cancer Lett, 2006.

7 Seong H, An TK, Khang G, Choi SU, Lee CO and Lee HB: BCNU-loaded poly(D, L-lactide-co-glycolide) wafer and antitumor activity against XF-498 human CNS tumor cells *in vitro*. Int J Pharm *251*: 1-12, 2003.

8 Lee JS, An TK, Chae GS, Jeong JK, Cho SH, Lee HB and Khang G: Evaluation of *in vitro* and *in vivo* antitumor activity of BCNU-loaded PLGA wafer against 9L gliosarcoma. Eur J Pharm Biopharm *59*: 169-175, 2005.

9 Westphal M, Hilt DC, Bortey E, Delavault P, Olivares R, Warnke PC, Whittle IR, Jaaskelainen J and Ram Z: A phase 3 trial of local chemotherapy with biodegradable carmustine (BCNU) wafers (Gliadel wafers) in patients with primary malignant glioma. Neuro-oncol *5*: 79-88, 2003.

10 Bobola MS, Silber JR, Ellenbogen RG, Geyer JR, Blank A and Goff RD: O6-methylguanine-DNA methyltransferase, O_6-benzylguanine, and resistance to clinical alkylators in pediatric primary brain tumor cell lines. Clin Cancer Res *11*: 2747-2755, 2005.

11 Hermisson M, Klumpp A, Wick W, Wischhusen J, Nagel G, Roos W, Kaina B and Weller M: O_6-methylguanine DNA methyltransferase and p53 status predict temozolomide sensitivity in human malignant glioma cells. J Neurochem *96*: 766-776, 2006.

12 Manome Y, Watanabe M, Futaki K, Ishiguro H, Iwagami S, Noda K, Dobashi H, Ochiai Y, Ohara Y, Sanuki K, Kunieda T and Ohno T: Development of a syngenic brain-tumor model resistant to chloroethyl-nitrosourea using a methylguanine DNA methyltransferase cDNA. Anticancer Res *19*: 5313-5318, 1999.

13 Manome Y, Yoshinaga H, Watanabe M and Ohno T: Adenoviral transfer of antisenses or ribozyme to O_6-methylguanine-DNA methyltransferase mRNA in brain-tumor model resistant to chloroethyl-nitrosourea. Anticancer Res *22*: 2029-2036, 2002.

14 Lesniak MS, Upadhyay U, Goodwin R, Tyler B and Brem H: Local delivery of doxorubicin for the treatment of malignant brain tumors in rats. Anticancer Res *25*: 3825-3831, 2005.

15 Webb AR, Yang J and Ameer GA: Biodegradable polyester elastomers in tissue engineering. Expert Opin Biol Ther *4*: 801-812, 2004.

16 Fonseca C, Simoes S and Gaspar R: Paclitaxel-loaded PLGA nanoparticles: preparation, physicochemical characterization and *in vitro* anti-tumoral activity. J Control Release *83*: 273-286, 2002.

17 Kang BK, Chon SK, Kim SH, Jeong S, Kim MS, Cho SH, Lee HB and Khang G: Controlled release of paclitaxel from microemulsion containing PLGA and evaluation of anti-tumor activity *in vitro* and *in vivo*. Int J Pharm *286*: 147-156, 2004.

18 Mo Y and Lim LY: Paclitaxel-loaded PLGA nanoparticles: potentiation of anticancer activity by surface conjugation with wheat germ agglutinin. J Control Release *108*: 244-262, 2005.

19 Mo Y and Lim LY: Preparation and *in vitro* anticancer activity of wheat germ agglutinin (WGA)-conjugated PLGA nanoparticles loaded with paclitaxel and isopropyl myristate. J Control Release. *107*: 30-42, 2005.

20 Sahoo SK and Labhasetwar V: Enhanced antiproliferative activity of transferrin-conjugated paclitaxel-loaded nanoparticles is mediated *via* sustained intracellular drug retention. Mol Pharm *2*: 373-383, 2005.

21 Lin R, Shi Ng L and Wang CH: *In vitro* study of anticancer drug doxorubicin in PLGA-based microparticles. Biomaterials *26*: 4476-4485, 2005.

22 Yoo HS and Park TG: Biodegradable polymeric micelles composed of doxorubicin conjugated PLGA-PEG block copolymer. J Control Release *70*: 63-70, 2001.

23 Mallery SR, Pei P, Kang J, Ness GM, Ortiz R, Touhalisky JE and Schwendeman SP: Controlled-release of doxorubicin from poly(lactide-co-glycolide) microspheres significantly enhances cytotoxicity against cultured AIDS-related Kaposi's sarcoma cells. Anticancer Res *20*: 2817-2825, 2000.

24 Inoue K, Onishi H, Kato Y, Michiura T, Nakai K, Sato M, Yamamichi K, Machida Y and Nakane Y: Comparison of intraperitoneal continuous infusion of floxuridine and bolus administration in a peritoneal gastric cancer xenograft model. Cancer Chemother Pharmacol *53*: 415-422, 2004.

25 Cegnar M, Premzl A, Zavasnik-Bergant V, Kristl J and Kos J: Poly(lactide-co-glycolide) nanoparticles as a carrier system for delivering cysteine protease inhibitor cystatin into tumor cells. Exp Cell Res *301*: 223-231, 2004.

26 Tong W, Wang L and D'Souza MJ: Evaluation of PLGA microspheres as delivery system for antitumor agent-camptothecin. Drug Dev Ind Pharm *29*: 745-756, 2003.

27 Roullin VG, Deverre JR, Lemaire L, Hindre F, Venier-Julienne MC, Vienet R and Benoit JP: Anti-cancer drug diffusion within living rat brain tissue: an experimental study using [^{3}H](6)-5-fluorouracil-loaded PLGA microspheres. Eur J Pharm Biopharm *53*: 293-299, 2002.

28 Hagiwara A, Sakakura C, Shirasu M, Yamasaki J, Togawa T, Takahashi T, Muranishi S, Hyon S and Ikada Y: Therapeutic effects of 5-fluorouracil microspheres on peritoneal carcinomatosis induced by Colon 26 or B-16 melanoma in mice. Anticancer Drugs *9*: 287-289, 1998.

29 Lagarce F, Cruaud O, Deuschel C, Bayssas M, Griffon-Etienne G and Benoit J: Oxaliplatin loaded PLAGA microspheres: design of specific release profiles. Int J Pharm *242*: 243-246, 2002.

30 Singh UV and Udupa N: *In vitro* characterization of methotrexate loaded poly(lactic-co-glycolic) acid microspheres and antitumor efficacy in Sarcoma-180 mice bearing tumor. Pharm Acta Helv *72*: 165-173, 1997.

31 Kumagai S, Sugiyama T, Nishida T, Ushijima K and Yakushiji M: Improvement of intraperitoneal chemotherapy for rat ovarian cancer using cisplatin-containing microspheres. Jpn J Cancer Res *87*: 412-417, 1996.

32 Waeckerle-Men Y and Groettrup M: PLGA microspheres for improved antigen delivery to dendritic cells as cellular vaccines. Adv Drug Deliv Rev *57*: 475-482, 2005.

33 Waeckerle-Men Y, Scandella E, Uetz-Von Allmen E, Ludewig B, Gillessen S, Merkle HP, Gander B and Groettrup M: Phenotype and functional analysis of human monocyte-derived dendritic cells loaded with biodegradable poly(lactide-co-glycolide) microspheres for immunotherapy. J Immunol Methods *287*: 109-124, 2004.

34 McCarthy JR, Perez JM, Bruckner C and Weissleder R: Polymeric nanoparticle preparation that eradicates tumors. Nano Lett *5*: 2552-2556, 2005.

35 Vargas A, Pegaz B, Debefve E, Konan-Kouakou Y, Lange N, Ballini JP, van den Bergh H, Gurny R and Delie F: Improved photodynamic activity of porphyrin loaded into nanoparticles: an *in vivo* evaluation using chick embryos. Int J Pharm *286*: 131-145, 2004.

36 Konan YN, Berton M, Gurny R and Allemann E: Enhanced photodynamic activity of meso-tetra(4-hydroxyphenyl)porphyrin by incorporation into sub-200 nm nanoparticles. Eur J Pharm Sci *18*: 241-249, 2003.

37 Konan YN, Chevallier J, Gurny R and Allemann E: Encapsulation of p-THPP into nanoparticles: cellular uptake, subcellular localization and effect of serum on photodynamic activity. Photochem Photobiol *77*: 638-644, 2003.

38 Geze A, Venier-Julienne MC, Saulnier P, Varlet P, Daumas-Duport C, Devauchelle P and Benoit JP: Modulated release of IdUrd from poly (D,L-lactide-co-glycolide) microspheres by addition of poly (D,L-lactide) oligomers. J Control Release *58*: 311-322, 1999.

39 Reza MS and Whateley TL: Iodo-2'-deoxyuridine (IUdR) and 125IUdR loaded biodegradable microspheres for controlled delivery to the brain. J Microencapsul *15*: 789-801, 1998.

40 Prabha S and Labhasetwar V: Critical determinants in PLGA/PLA nanoparticle-mediated gene expression. Pharm Res *21*: 354-364, 2004.

41 Jilek S, Ulrich M, Merkle HP and Walter E: Composition and surface charge of DNA-loaded microparticles determine maturation and cytokine secretion in human dendritic cells. Pharm Res *21*: 1240-1247, 2004.

42 Panyam J, Zhou WZ, Prabha S, Sahoo SK and Labhasetwar V: Rapid endo-lysosomal escape of poly(DL-lactide-co-glycolide) nanoparticles: implications for drug and gene delivery. Faseb J *16*: 1217-1226, 2002.

43 Gill JS, Zhu X, Moore MJ, Lu L, Yaszemski MJ and Windebank AJ: Effects of NFkappaB decoy oligonucleotides released from biodegradable polymer microparticles on a glioblastoma cell line. Biomaterials *23*: 2773-2781, 2002.

44 Benny O, Duvshani-Eshet M, Cargioli T, Bello L, Bikfalvi A, Carroll RS and Machluf M: Continuous delivery of endogenous inhibitors from poly(lactic-co-glycolic acid) polymeric microspheres inhibits glioma tumor growth. Clin Cancer Res *11*: 768-776, 2005.

45 Bandi N, Ayalasomayajula SP, Dhanda DS, Iwakawa J, Cheng PW and Kompella UB: Intratracheal budesonide-poly(lactide-co-glycolide) microparticles reduce oxidative stress, VEGF expression, and vascular leakage in a benzo(a)pyrene-fed mouse model. J Pharm Pharmacol *57*: 851-860, 2005.

46 Ribeiro-Costa RM, Alves AJ, Santos NP, Nascimento SC, Goncalves EC, Silva NH, Honda NK and Santos-Magalhaes NS: *In vitro* and *in vivo* properties of usnic acid encapsulated into PLGA-microspheres. J Microencapsul *21*: 371-384, 2004.

47 Sanchez A, Tobio M, Gonzalez L, Fabra A and Alonso MJ: Biodegradable micro- and nanoparticles as long-term delivery vehicles for interferon-alpha. Eur J Pharm Sci *18*: 221-229, 2003.

48 Ferdous AJ, Stembridge NY and Singh M: Role of monensin PLGA polymer nanoparticles and liposomes as potentiator of ricin A immunotoxins *in vitro*. J Control Release *50*: 71-78, 1998.

49 Jeong YI, Song JG, Kang SS, Ryu HH, Lee YH, Choi C, Shin BA, Kim KK, Ahn KY and Jung S: Preparation of poly(DL-lactide-co-glycolide) microspheres encapsulating all-trans retinoic acid. Int J Pharm *259*: 79-91, 2003.

50 Labrie F, Li S, Belanger A, Cote J, Merand Y and Lepage M: Controlled release low dose medroxyprogesterone acetate (MPA) inhibits the development of mammary tumors induced by dimethyl-benz(a) anthracene in the rat. Breast Cancer Res Treat *26*: 253-265, 1993.

51 Chae GS, Lee JS, Kim SH, Seo KS, Kim MS, Lee HB and Khang G: Enhancement of the stability of BCNU using self-emulsifying drug delivery systems (SEDDS) and *in vitro* antitumor activity of self-emulsified BCNU-loaded PLGA wafer. Int J Pharm 301: 6-14, 2005.

52 Rohr UD, Oberhoff C, Markmann S, Gerber B, Scheulen M and Schindler AE: The safety of synthetic paclitaxel by intralesional delivery with OncoGeltrade mark into skin breast cancer metastases: method and results of a clinical pilot trial. Arch Gynecol Obstet 1-7, 2005.

53 Fournier C, Hecquet B, Bouffard P, Vert M, Caty A, Vilain MO, Vanseymortier L, Merle S, Krikorian A, Lefebvre JL *et al*: Experimental studies and preliminary clinical trial of vinorelbine-loaded polymeric bioresorbable implants for the local treatment of solid tumors. Cancer Res *51*: 5384-5391, 1991.

54 Jordan B, Pasquier Y and Schnider A: Neurological improvement and rehabilitation potential following toxic myelopathy due to intrathecal injection of doxorubicin. Spinal Cord *42*: 371-373, 2004.

55 Arico M, Nespoli L, Porta F, Caselli D, Raiteri E and Burgio GR: Severe acute encephalopathy following inadvertent intrathecal doxorubicin administration. Med Pediatr Oncol *18*: 261-263, 1990.

Received May 5, 2006
Accepted May 29, 2006

MRIの優位性はここにある

外科手術に効果大きいMR設置のMRX手術室開設と応用開始

国立がんセンター
小林寿光　中馬広一　木下貴之　宮北康二
山崎直也　下山直人　土屋了介　垣添忠生

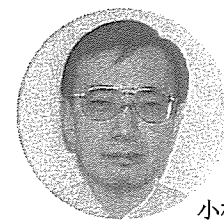
小林氏

要旨：画像装置を手術中に使用することで、標準的な外科成果に上乗せ効果を期待した、MRIやCT、フラットパネルX線透視装置を導入した新たな手術室、MRX手術室が開設され、臨床試験として応用が開始された。

MRI装置の手術室導入で目指す手術の標準化と低侵襲化

外科治療は悪性腫瘍の治癒が期待できる標準的な治療法であるが、高度な手術技術の標準化と標準的な手術の低侵襲化は重要な課題である。

一般に熟練した外科医でも難しいのは、体内深部の狭小部、また見えづらい領域であり、経験に基づく高い技術が必要である。単なる勘に頼って無理をすれば、効果と安全性が犠牲になる可能性があった。

MRX手術室開発の目的は上乗せ効果

画像装置は病変の発見から診断、手術適応の決定に使用されており、手術中に使用できれば何らかの上乗せ効果が期待される。手術を中心に考えれば画像診断室で手術ができる設備を整えるのではなく、これまでの手術室環境を保ったまま画像装置を導入する必要がある。

確かに画像装置を使用した新たな放射線科的な医療技術開発[1,2]や、脳神経外科などの医療技術を高度化することには非常に大きな意義がある[3,4]。しかし医療施設全体として導入経費と成果のバランスを取るためには、幅広い外科領域に対する汎用手術室として構築する必要がある。

以上の必要性から、新たな画像補助手術室は、既存の手術室フロアの一角に導入されることとなった。

手術室に導入する画像機器装置はMRIにCT、FPD

導入する画像装置は手術適応を決定するために使用されるものの中で、手術室の建設時に設置が必要なMRIとCT、X線透視装置とした。基準とするものを最も導入が難しいMRIとして、できるだけ幅広い周囲からアプローチできるオープン型とした。当初は軽量の0・2Tモデルを考えていたが、広いガントリー開口部上下幅（43㎝）を得るために0・3Tモデルとした。

CTはMRIと必要に応じて同期して運用することにも配慮したが、撮影時に術野や外科医の移動のみならず、麻酔などの配管や点滴ライン、心電図などのケーブルのつながった患者の移動を避けるために、自走式のマルチスライス（4列）ヘリカルCTを選定した。

●Summary
A new operating room, the MRX Surgical Room, which encompasses an MRI, CT and flatpanel fluoroscopy systems, in anticipation of increasing effectiveness with regard to the results of standard surgical procedures by using imaging systems intraoperatively, has begun functioning in clinical studies.

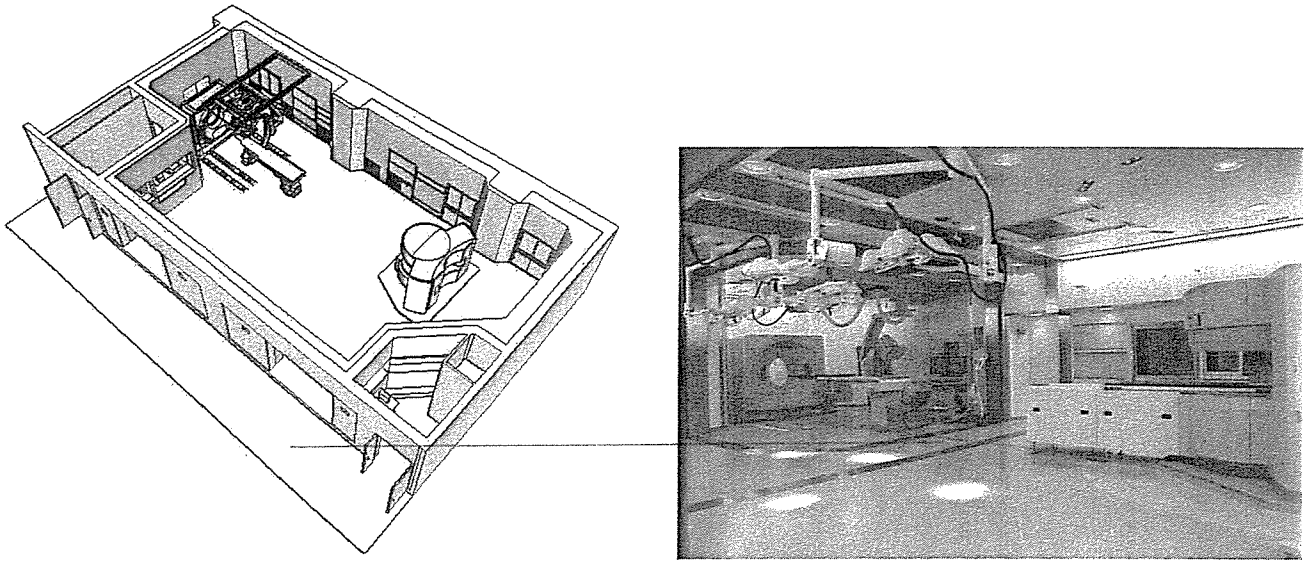

図1　右はMRX手術室、左は同手術室の3次元イメージ図

X線透視装置はこれまでも術中に使用されてきたが、コンパクトでコーンビームCTが可能なフラットパネルX線透視装置（FPD）とした。この装置はCT装置と検査・手術台を共有して、いわゆるIVR-CT/Angio装置の形態をとることとした。

共用手術スペースの確保の鍵は開閉式電磁波シールドカーテンの開発

MRIへの電磁波干渉を防止するには通常X線系装置を別室に配置するが、限られたスペース内で十分な手術スペースの確保が難しくなり、また全身麻酔下の患者移動にリスクが発生する。画像装置をすべて同室に設置した場合、X線系装置の電源を落とせば電磁波干渉を防止できるが、CTの立ち上げ時にキャリブレーションによる放射線被曝の問題等が発生する。そこでこれらX線系装置を囲み込む、開閉式電磁波シールドカーテンを開発することとした。

これを前提にしてMRI装置とX線系装置を手術室内の左右、入り口の反対側に寄せて設置することで、中央に広い共用手術スペースを確保した。将来この手術室の中央を開閉式間仕切りで分けて2室運用する可能性も考え、それぞれの操作室は左右に分けて設置することとした。

大問題なのは診療業務中に導入工事を行うこと

以上の計画からMRIの重量は約16トンで、手術室の総重量は約40トンに至ることが確認された。問題は当センター中央病院の床の耐荷重であり、床補強が建物の設計上可能であるかは大きな懸案であった。これは柱の間に設置された主梁を中心に、H鋼による補強を行うことで対処可能と計算され、結果として床面は25cm挙上された。また40トンの重量が19階建ての建物全体に及ぼす影響も、特に問題がないことが計算上確認された。

実際の導入工事を行う点で大きな問題は、病院が診療業務中であることである。各種工事区画や必要な人材、資材の出入りは患者動線に支障を与え、工事に伴う振動や騒音は隣接する手術室や階下のICUへの影響が懸念された。特に手術室は最も活性度の高い病院機能を持ち、各種医療ガスや信号配線、電源等に関連して、病院全体に影響し得ることが問題であった。

そこで手術フロアを含め工事区画を仕切り、器材の搬入を含めたエレベーター等の動線を患者診療用と離して設置した。また騒音、振動に関しては代表的な作業を極短時間シミュレーションしてその程度を評価したが、機器や工法の工夫で絶対量を抑えるとともに、土日の施工や部屋の適切な運用で対処が可能となった。また安全に最大限配慮した工事計画を作成することはもとより、万が一の事態を想定した高度なリスクマネージメントプランを作成し、単なる研究班のみならず病院組織との連携をとることで導入工事を進めた。

重量のあるMRIの搬入は通常のエレベーターが使用できないため、病院に併置して9